Electronic Supporting Information (ESI†)

Ni, Pd, and Pt Complexes of a Tetradentate Dianionic Thiosemicarbazone-Based O^N^N^S Ligand

Alexander Haseloer, Luca Mareen Denkler, Rose Jordan, Max Reimer, Selina Olthoff, Ines Schmidt, Klaus Meerholz, Gerald Hörner* and Axel Klein*

Contents

Table S2 Computed metrics of the complexes **[M(tBuL)]** (M = Ni, Pd, Pt) and the reference complex **F**.
Table S3 Selected DFT calculated structural parameters of **[M(L)]** and **[M(tBuL)]** (M = Ni, Pd or Pt).
Table S4 Absorption maxima of the protoligands **H_2L** and **H_2tBuL** and the complexes **[M(L)]** and **[M(tBuL)]** (M = Ni, Pd, Pt)
Table S5 (six tables) TD-DFT calculated absorptions of **[M(L)]** and **[MtBuL)]** M = Ni, Pd, Pt.
Table S6 Selected electrochemical data of the protoligands **H_2L** and **H_2tBuL** and the complexes **[M(L)]** and **[M(tBuL)]** (M = Ni, Pd, Pt).

Supporting Figures:

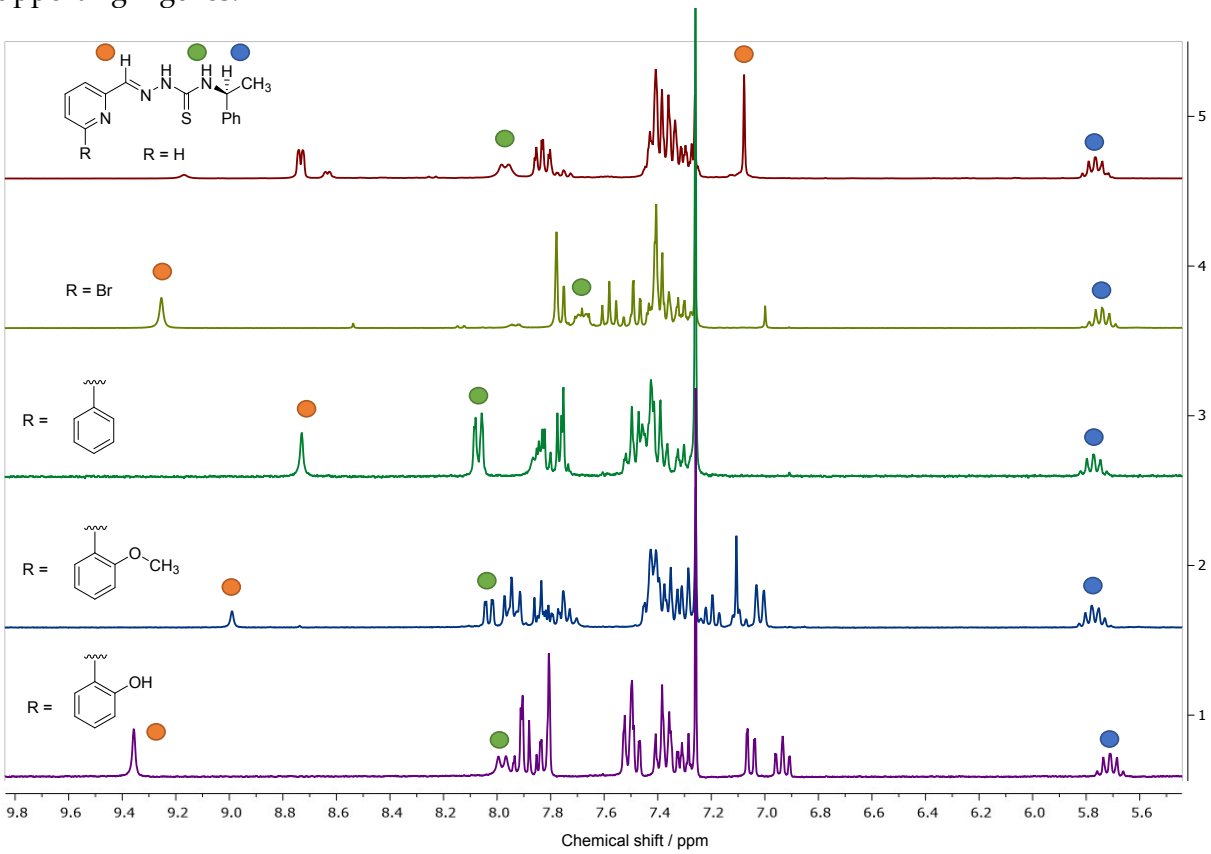

Fig. S1 400 MHz ^{1}H NMR spectra of **HL** and starting materials in $CDCl_3$. The imine proton is marked in orange, the amine proton is marked in green and the proton at the chiral carbon atom is marked in blue.

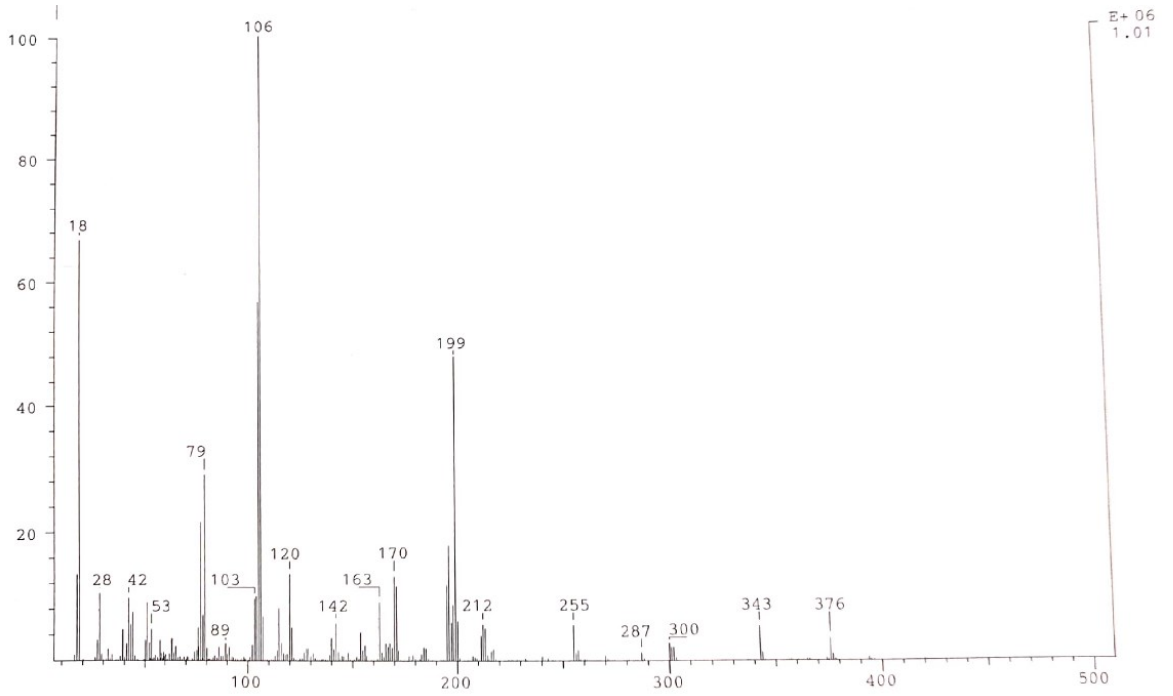

Fig. S2 EI-MS(+) of $\mathbf{H_2L}$.

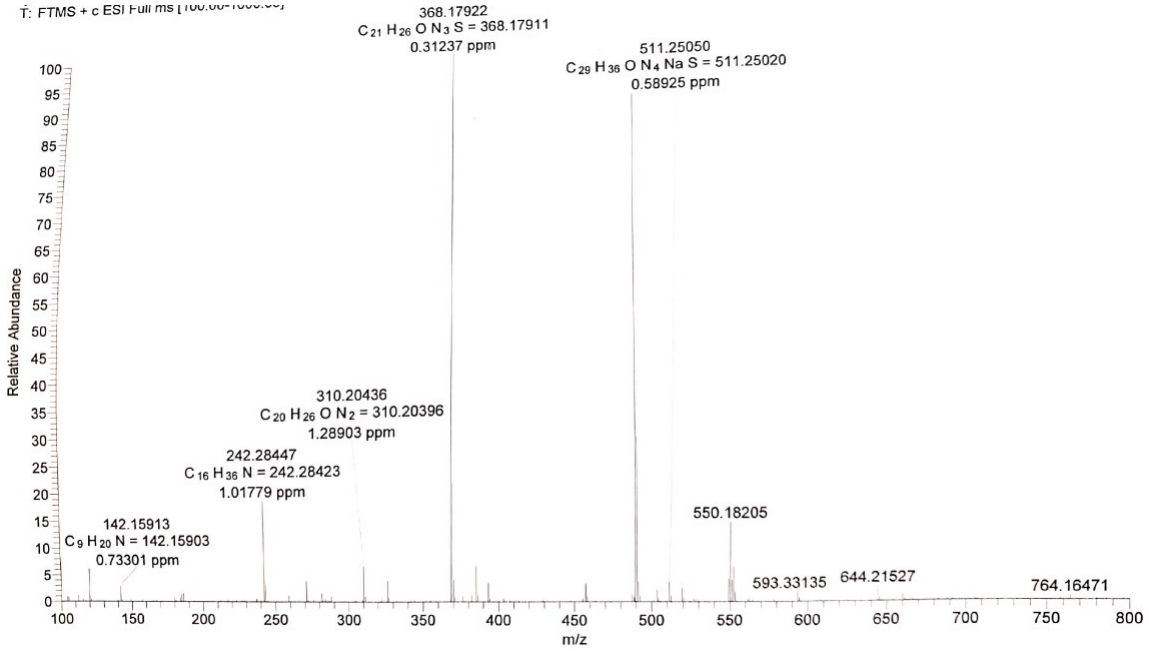

Fig. S3 HR-ESI-MS(+) of $\mathbf{H_2}^{\mathbf{tBu}}\mathbf{L}$.

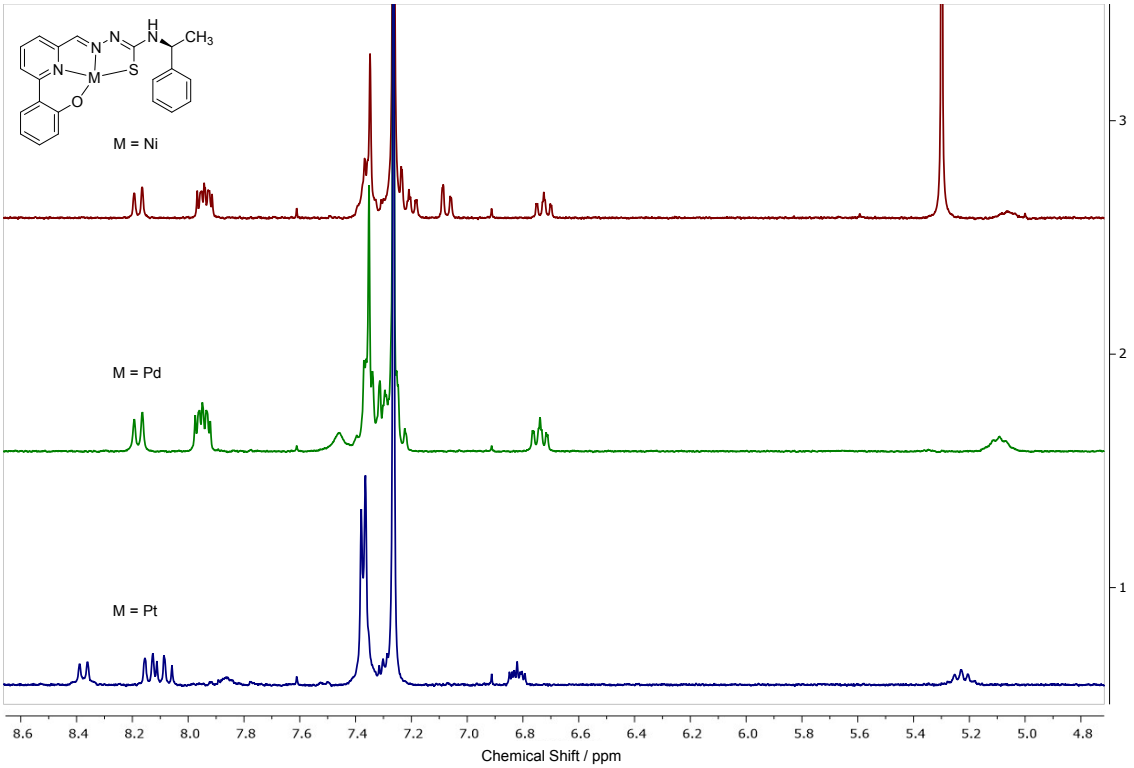

Fig. S4 400 MHz ^{1}H NMR spectra of **[Ni(L)]** (red), **[Pd(L)]** (green) and **[Pt(L)]** (blue) in DMSO-d_6.

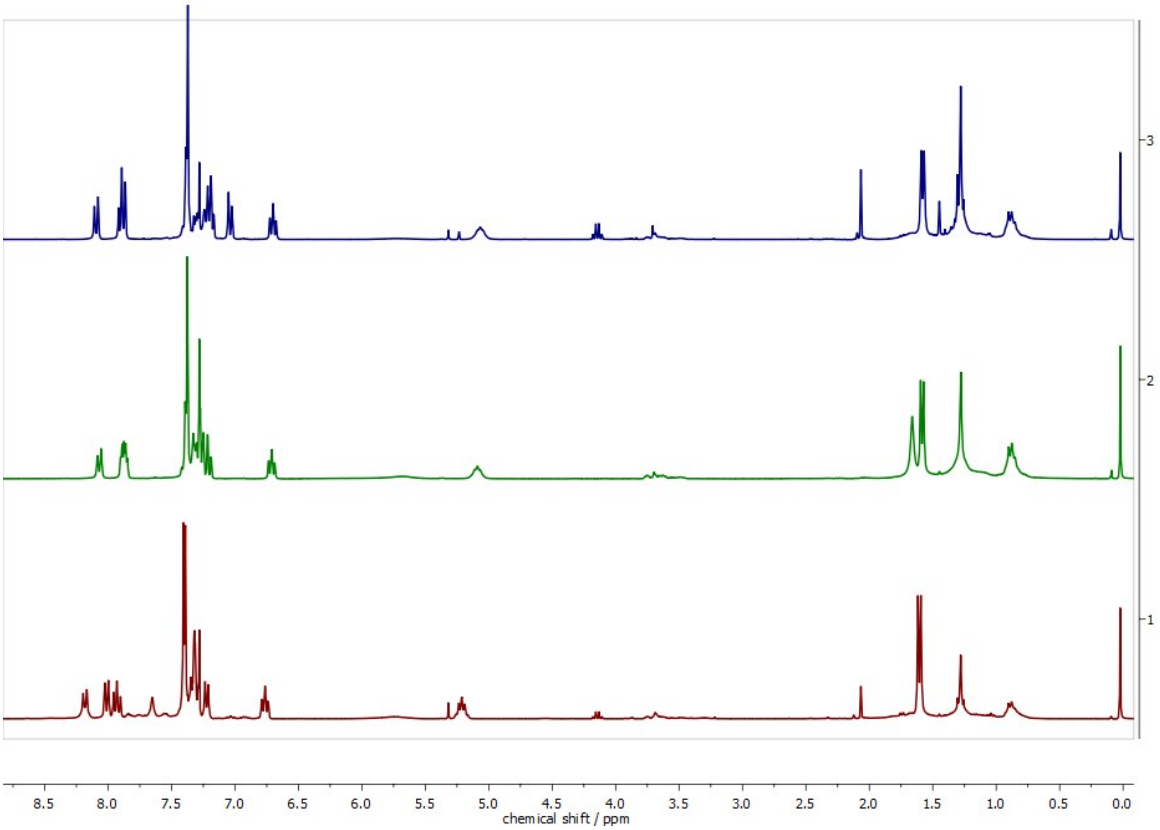

Fig. S5 400 MHz ^{1}H NMR spectra of **[Ni(L)]** (blue), **[Pd(L)]** (green), and **[Pt(L)]** (red) in $CDCl_3$.

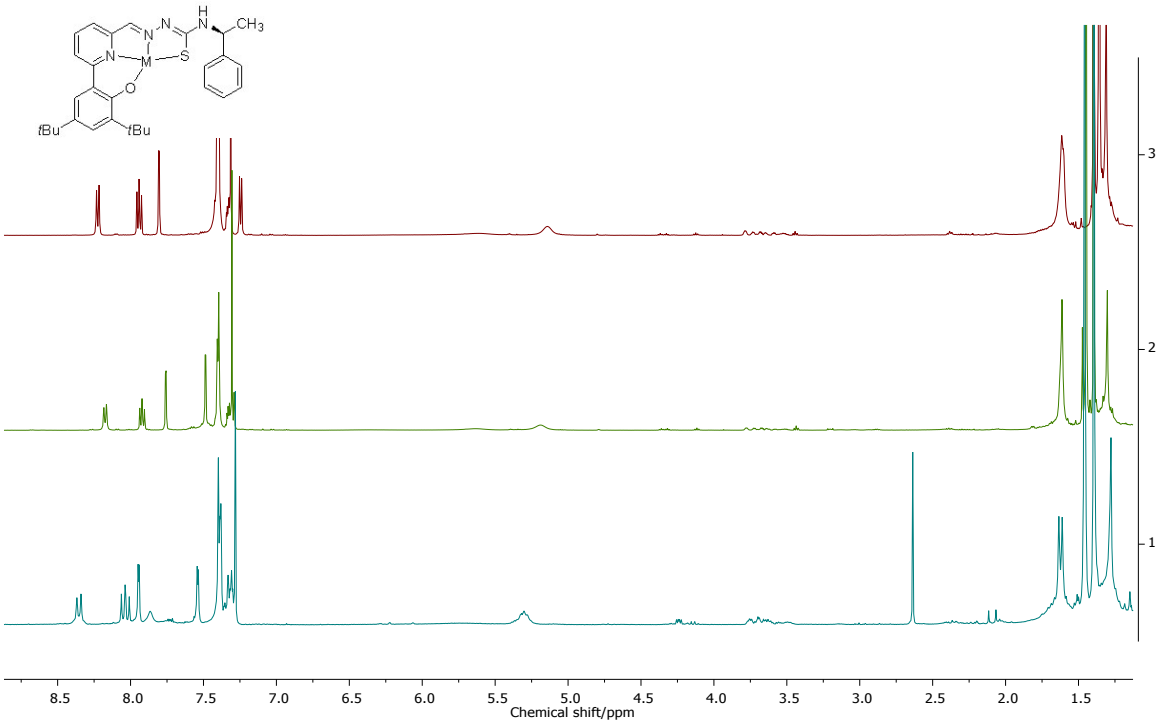

Fig. S6 300 MHz ^{1}H NMR spectra of **[Ni(^{tBu}L)]**, **[Pd(^{tBu}L)]**, and **[Pt(^{tBu}L)]** in $CDCl_3$.

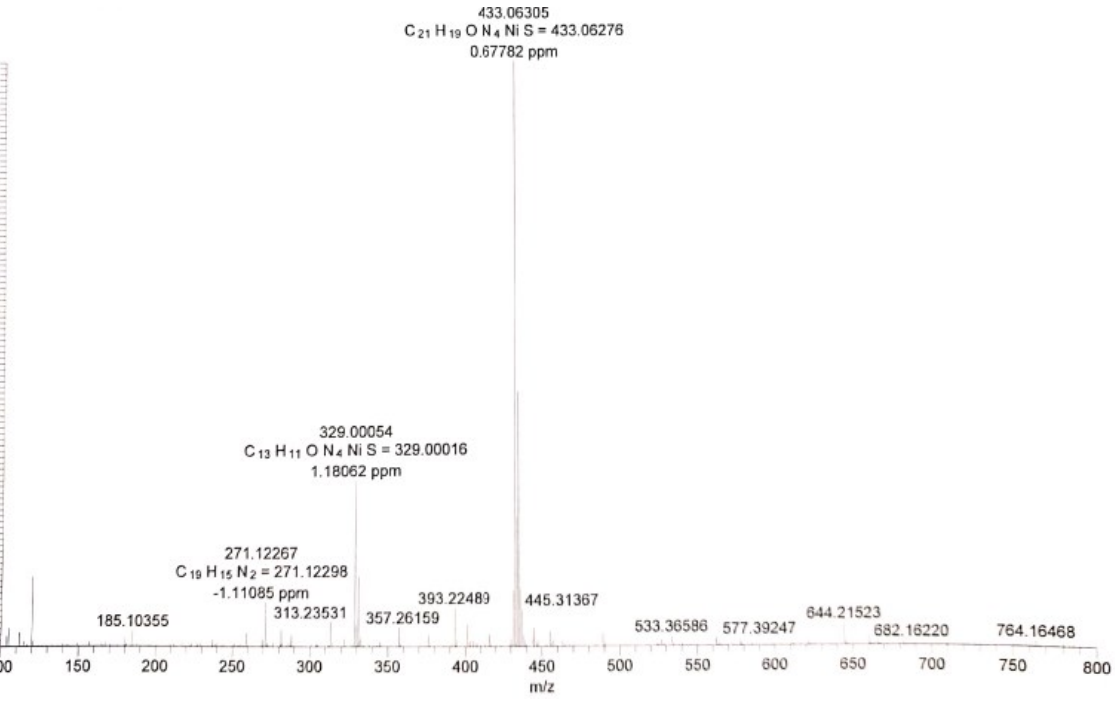

Fig. S7 HR-ESI-MS(+) of **[Ni(L)].**

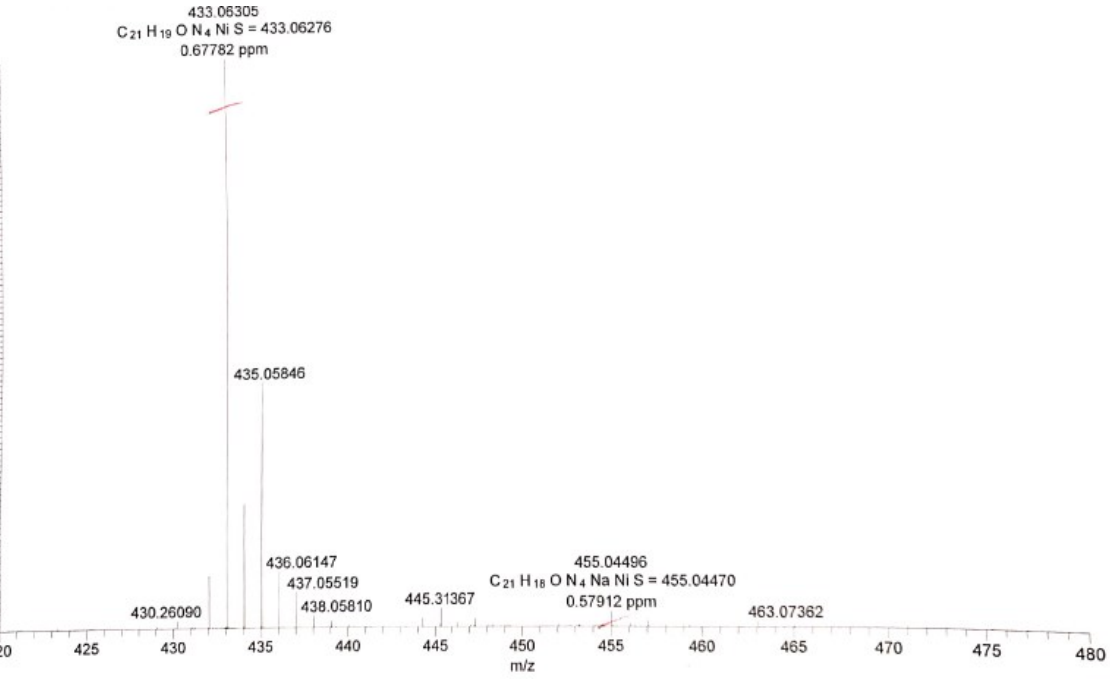

Fig. S8 Part of HR-ESI-MS(+) of **[Ni(L)]** showing $[M+H]^+$ (433 m/z) and $[M+Na]^+$ (455 m/z).

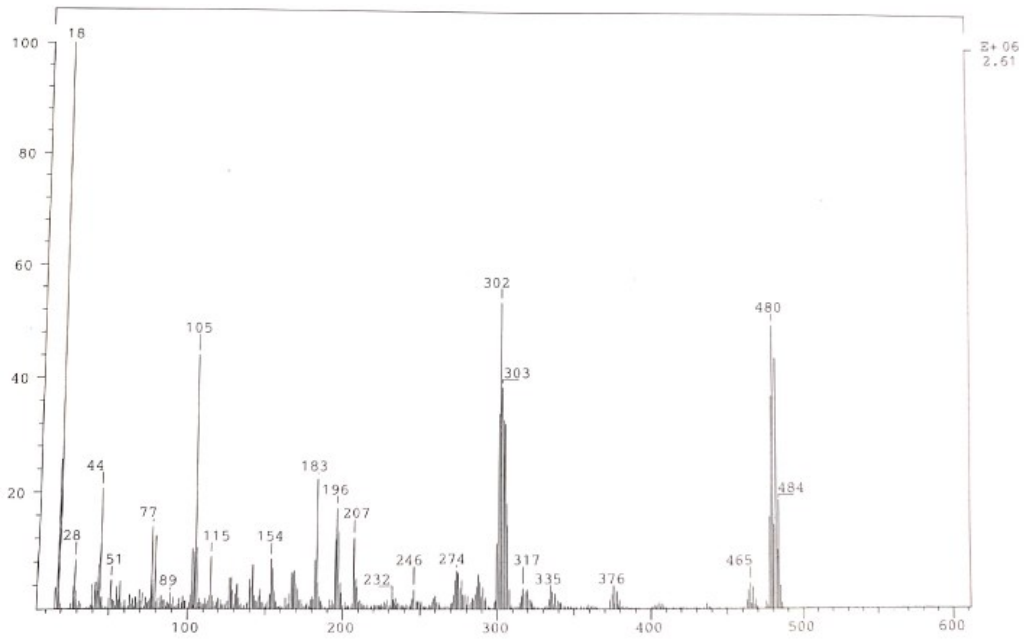

Fig. S9 EI-MS(+) of **[Pd(L)]**.

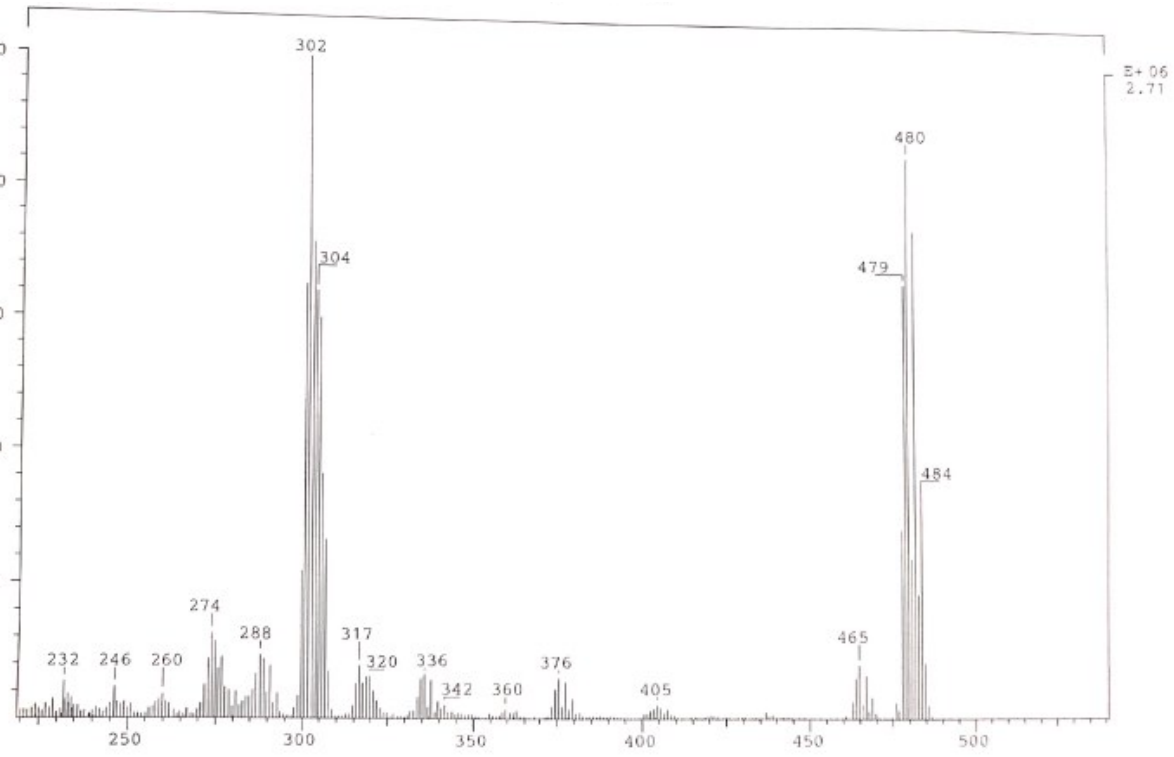

Fig. S10 Part of EI-MS(+) of **[Pd(L)]**.

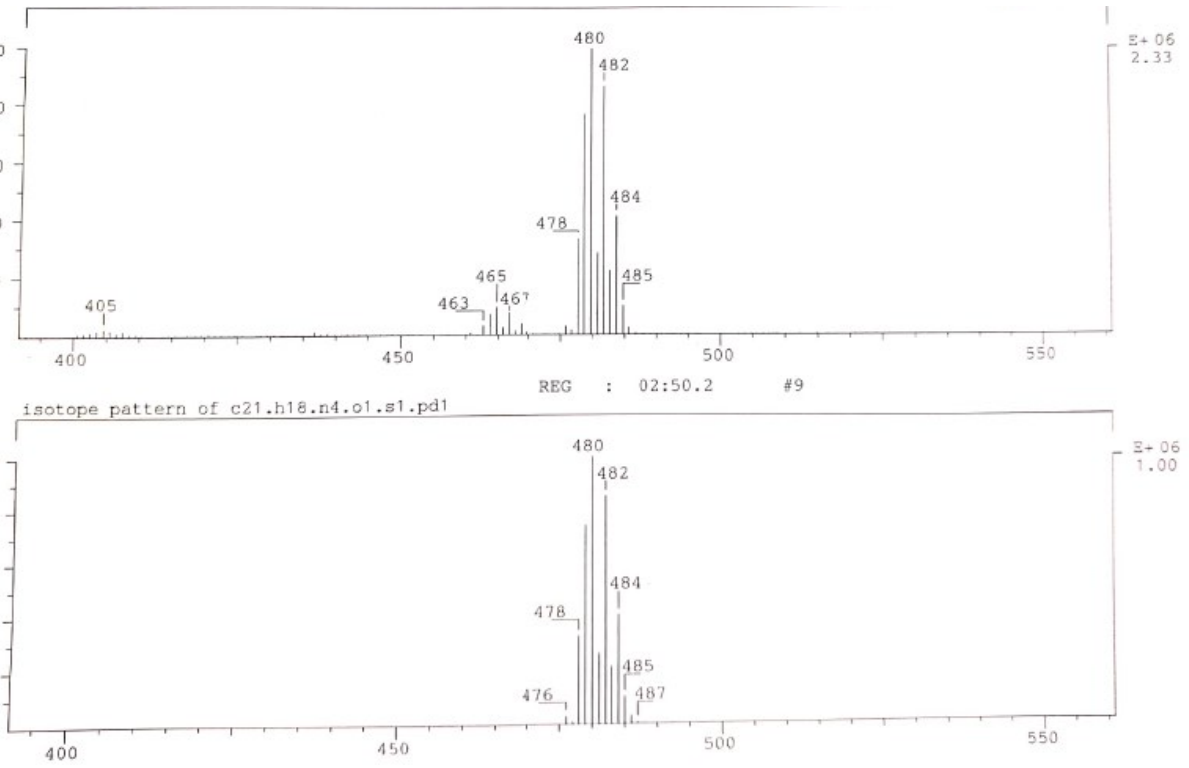

Fig. S11 EI-MS(+) molecular peak of **[Pd(L)]** (top) representing $[M]^+$ (480 m/z) and $[M\text{-}CH_3]^+$ (465 m/z) and calculated isotopic pattern for $[M]^+$ (bottom).

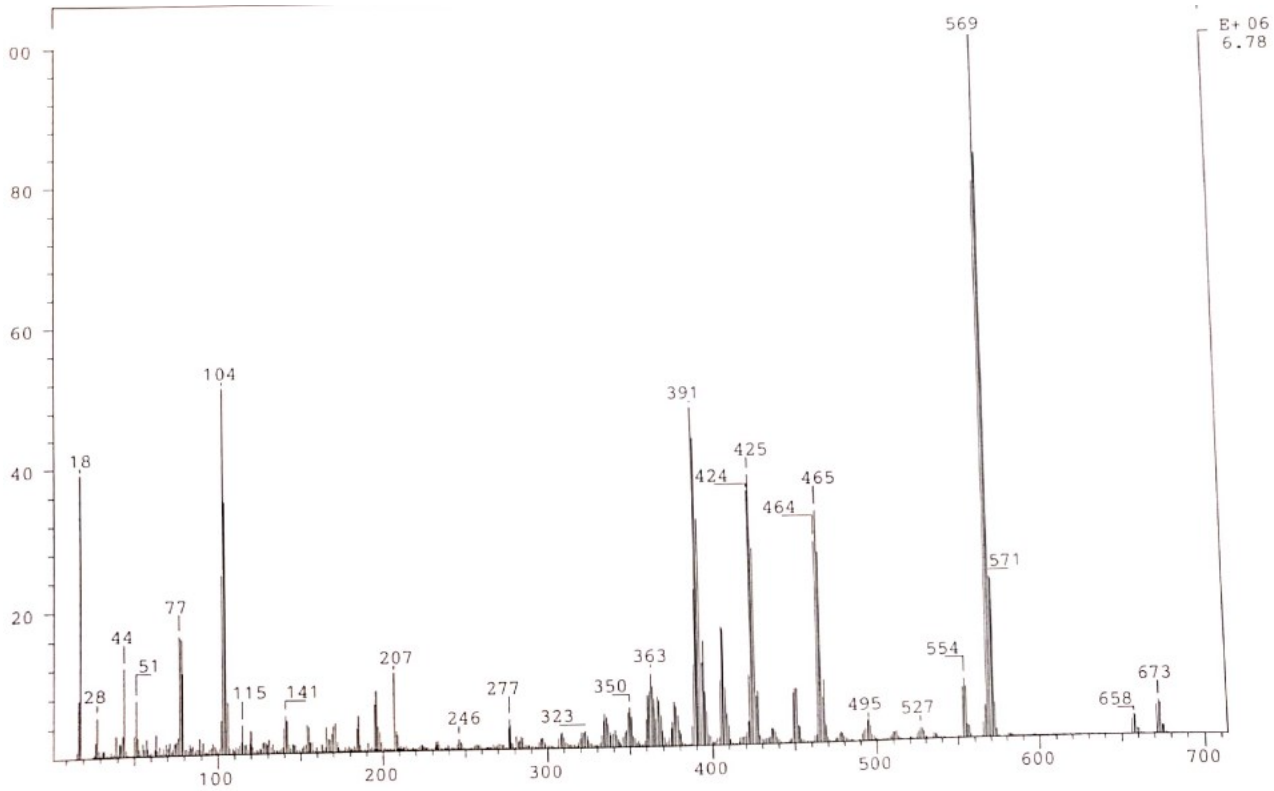

Fig. S12 EI-MS(+) of **[Pt(L)].**

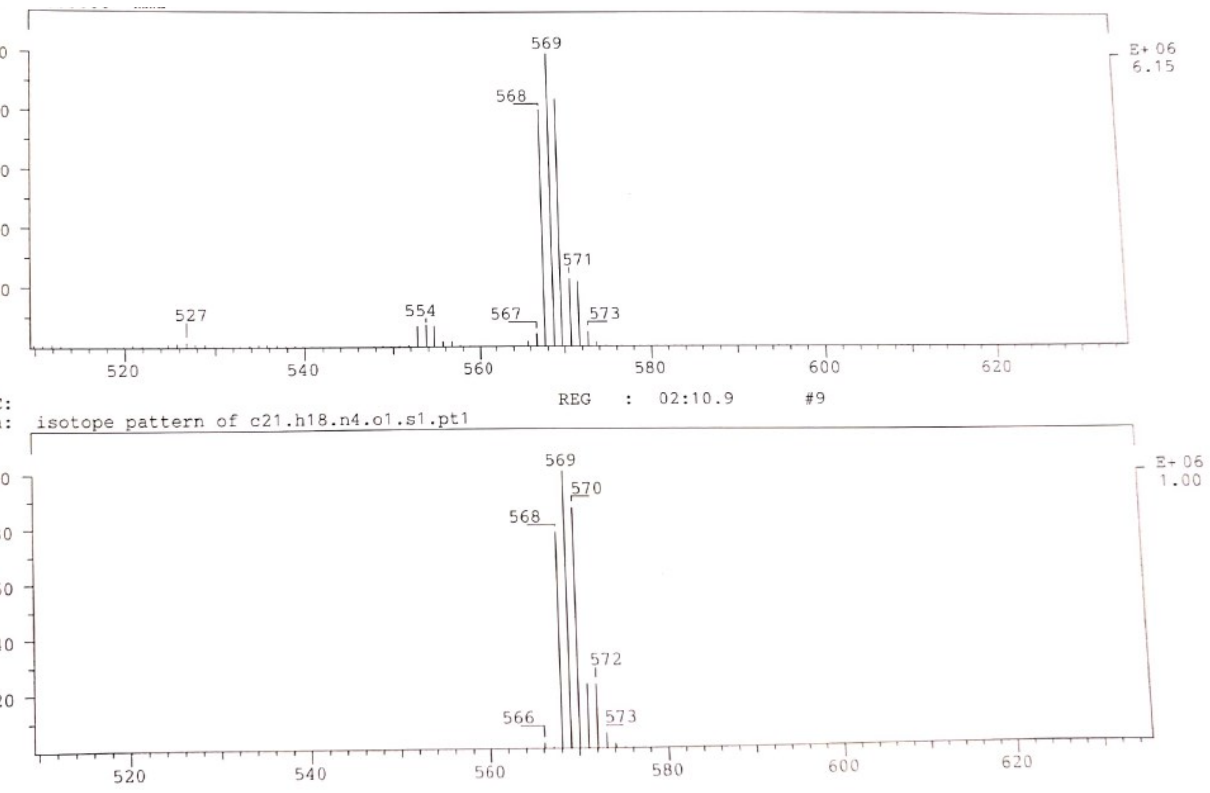

Fig. S13 EI-MS(+) molecular peaks of **[Pt(L)]** (top) representing $[M]^+$ at 569 m/z and calculated isotopic pattern (bottom).

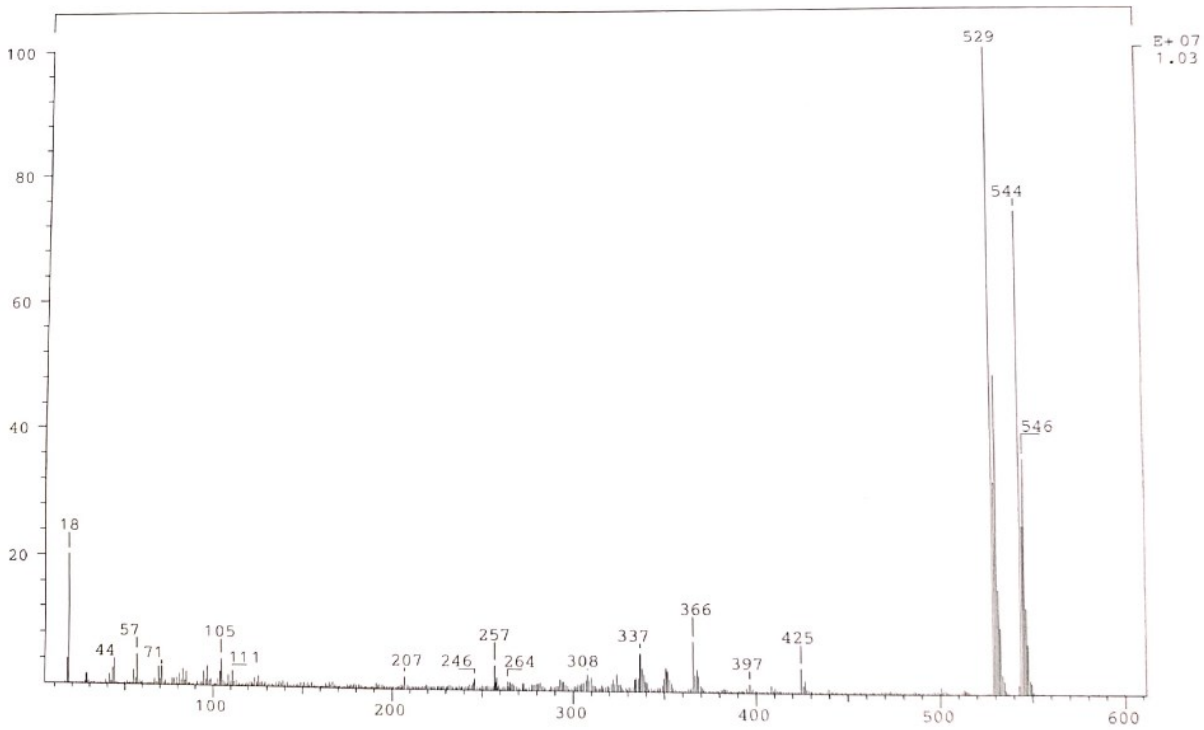

Fig. S14 EI-MS(+) of **[Ni(^tBuL)].**

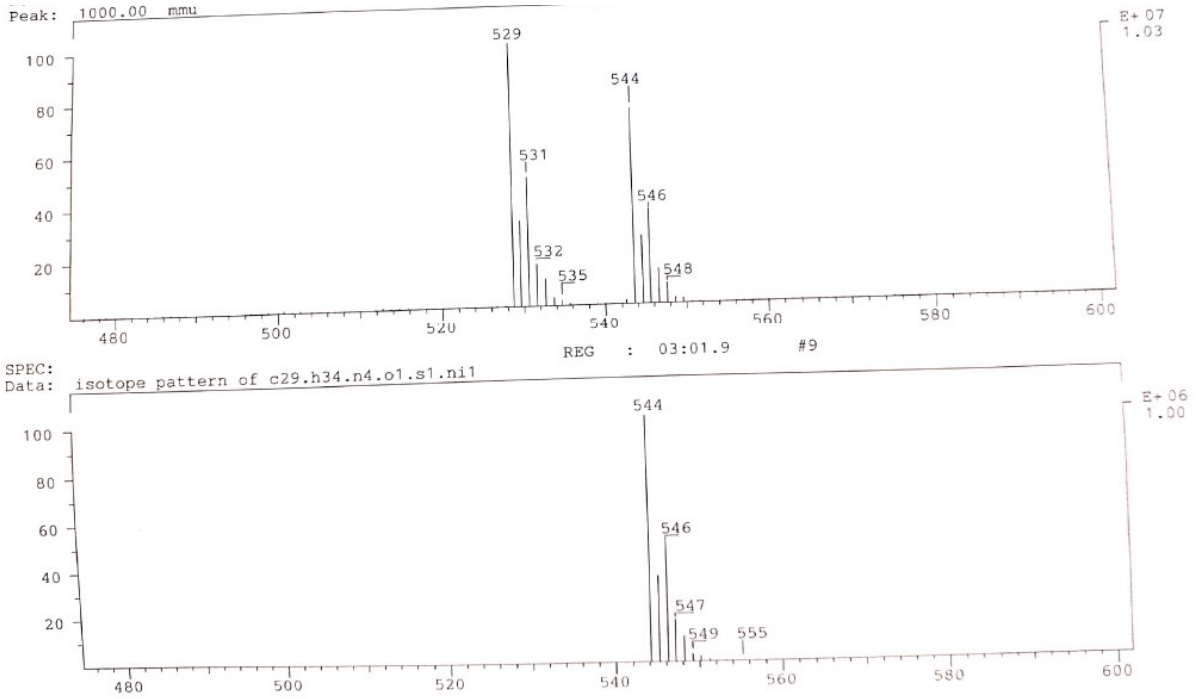

Fig. S15 EI-MS(+) molecular peaks of **[Ni(^tBuL)]** (top), representing $[M]^+$ (544 m/z) and $[M\text{-}CH_3]^+$ (529 m/z) and calculated isotopic pattern of $[M]^+$ (bottom).

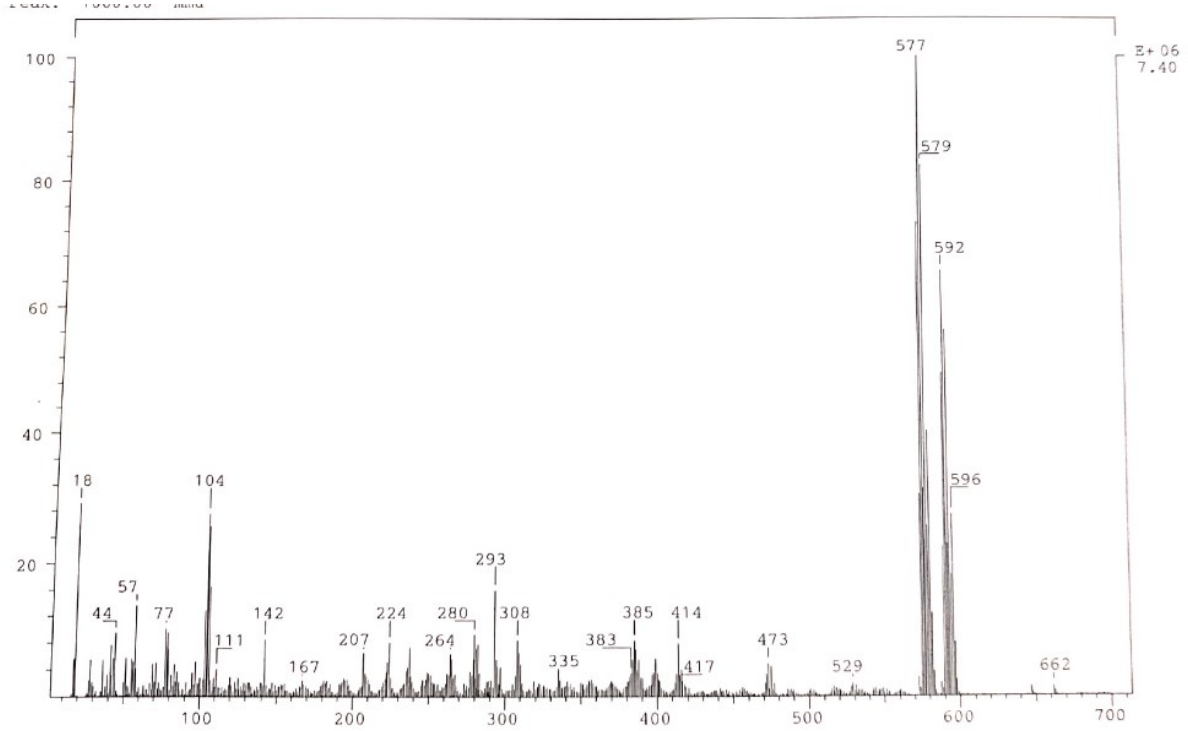

Fig. S16 EI-MS(+) of **[Pd(^tBuL)]**.

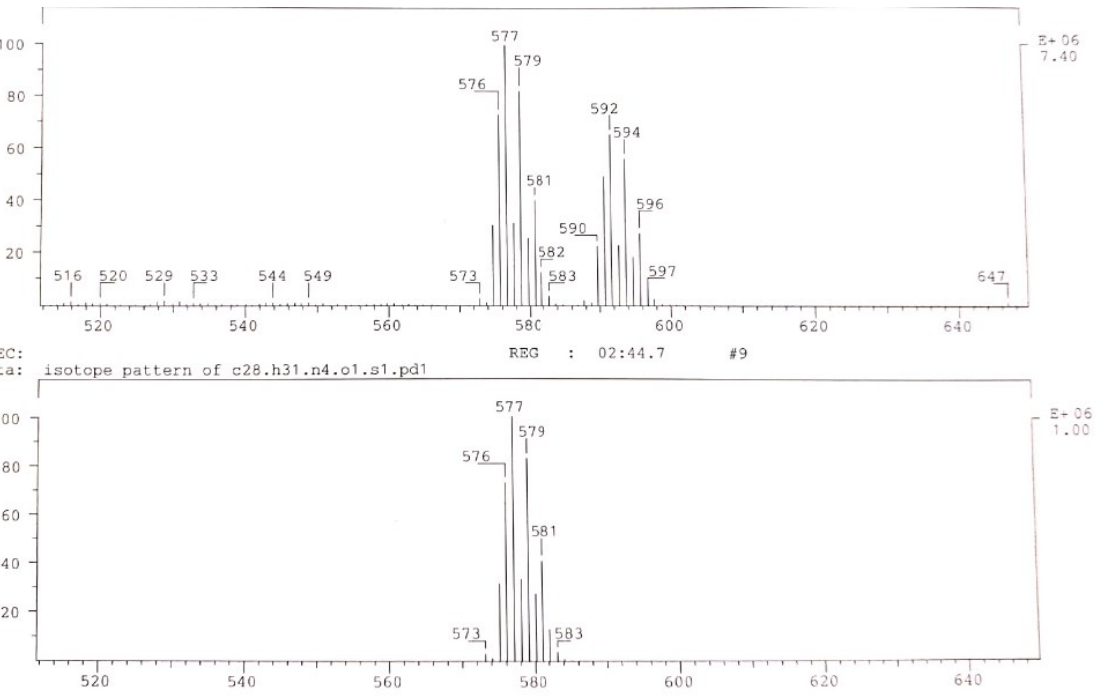

Fig. S17 EI-MS(+) molecular peaks of **[Pd(^tBuL)]** (top) representing $[M]^+$ (592 m/z) and $[M\text{-}CH_3]^+$ (577 m/z) and calculated isotopic pattern of $[M\text{-}CH_3]^+$.

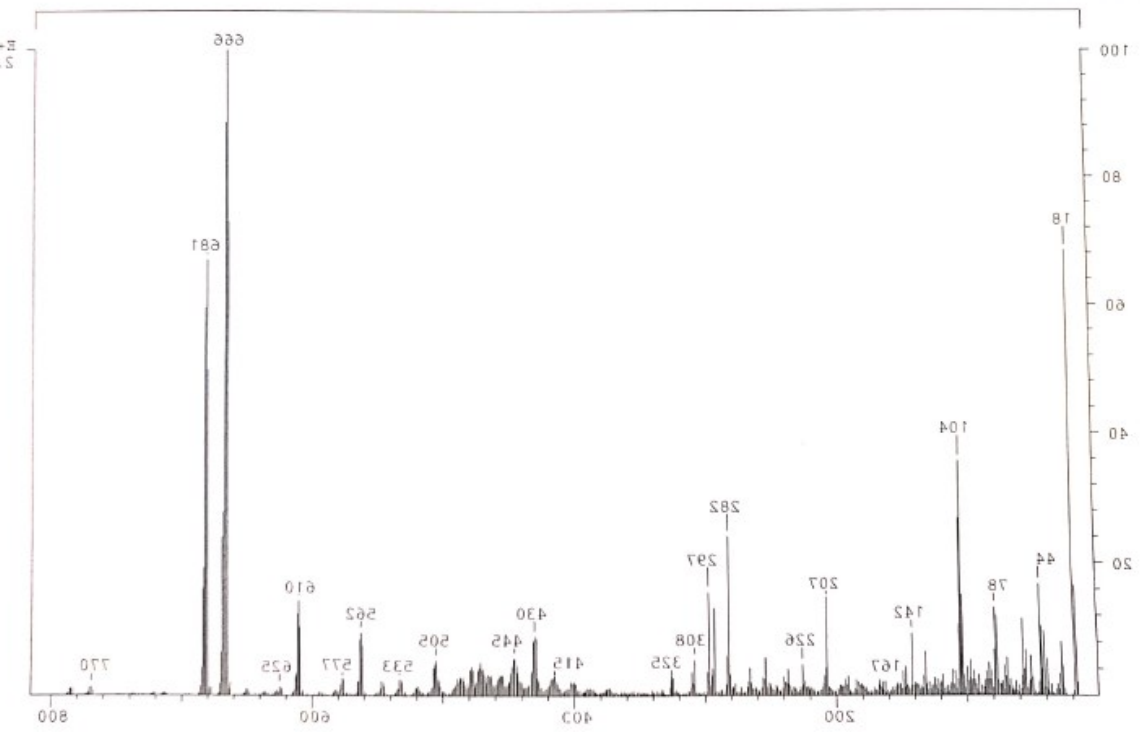

Fig. S18 EI-MS(+) of **[Pt(^{tBu}L)]**.

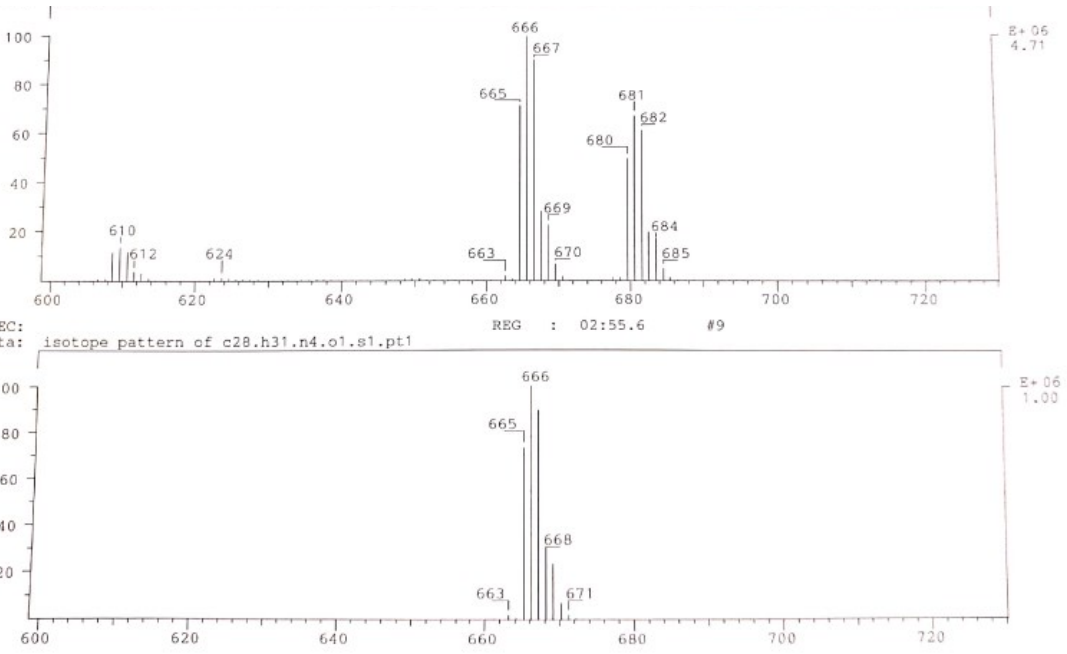

Fig. S19 EI-MS(+) molecular peak of **[Pt(**^{tBu}**L)]** representing $[M]^+$ (544 m/z) and $[M\text{-}CH_3]^+$ (529 m/z) and calculated isotopic pattern for $[M\text{-}CH_3]^+$ (bottom).

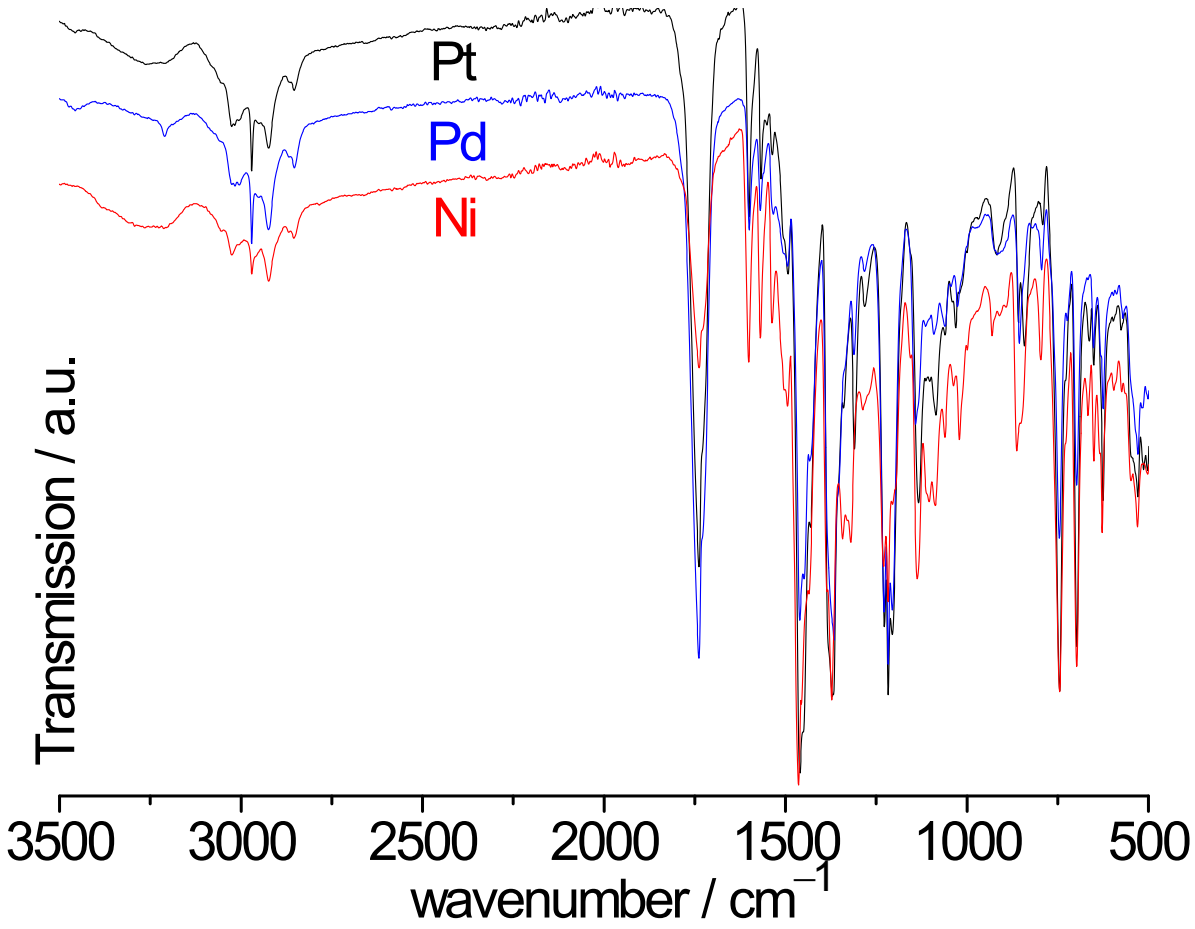

Fig. S20 IR spectra of **[Ni(L)]** (red), **[Pd(L)]** (blue), and **[Pt(L)]** (black).

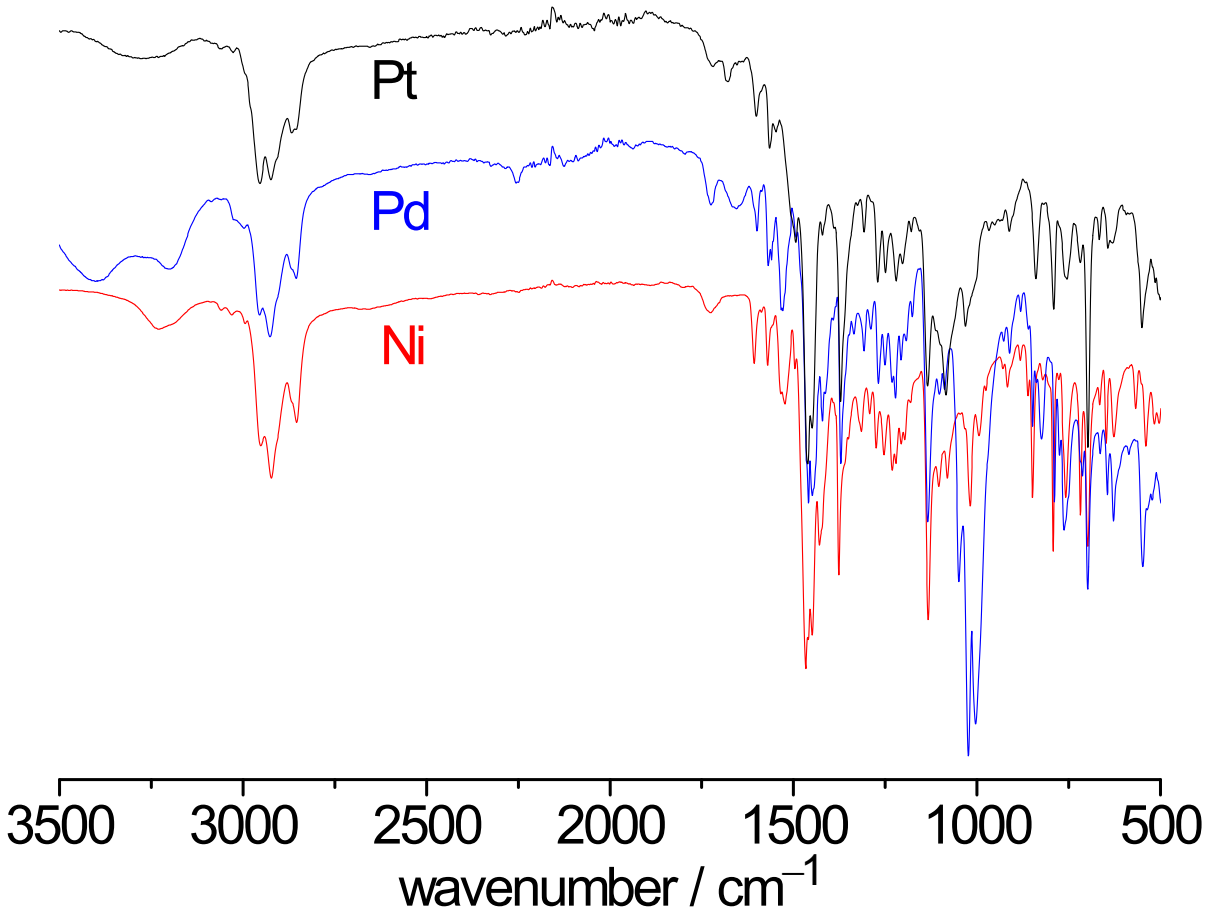

Fig. S21 IR spectra of **[Ni(ᵗᴮᵘL)]** (red), **[Pd(ᵗᴮᵘL)]** (blue), and **[Pt(ᵗᴮᵘL)]** (black).

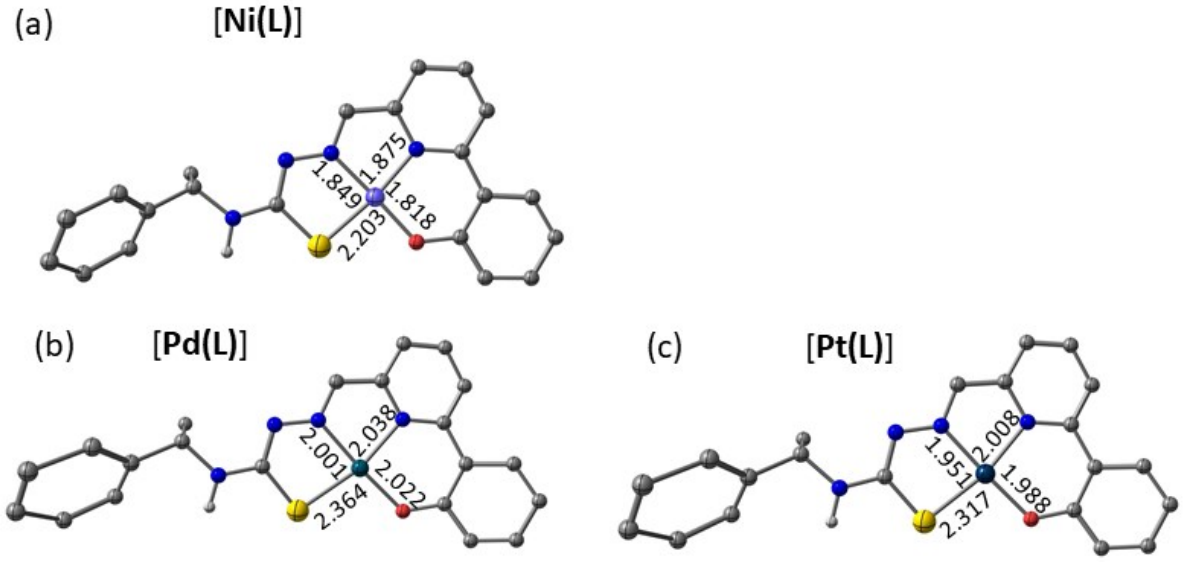

Fig. S22 Optimised structures and selected bond lengths of the complexes [**M(L)**] with M = Ni (a), Pd (b) and Pt (c).

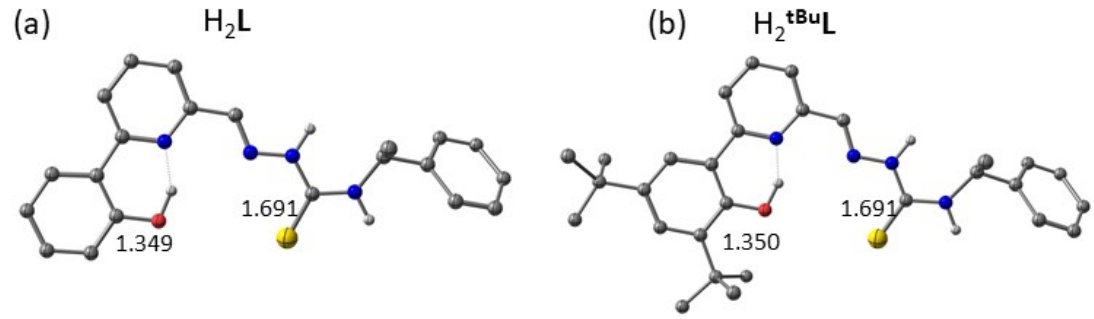

Fig. S23 Optimised structures and selected bond lengths of the protoligands $\mathbf{H_2L}$ (a) and $\mathbf{H_2^{tBu}L}$ (b).

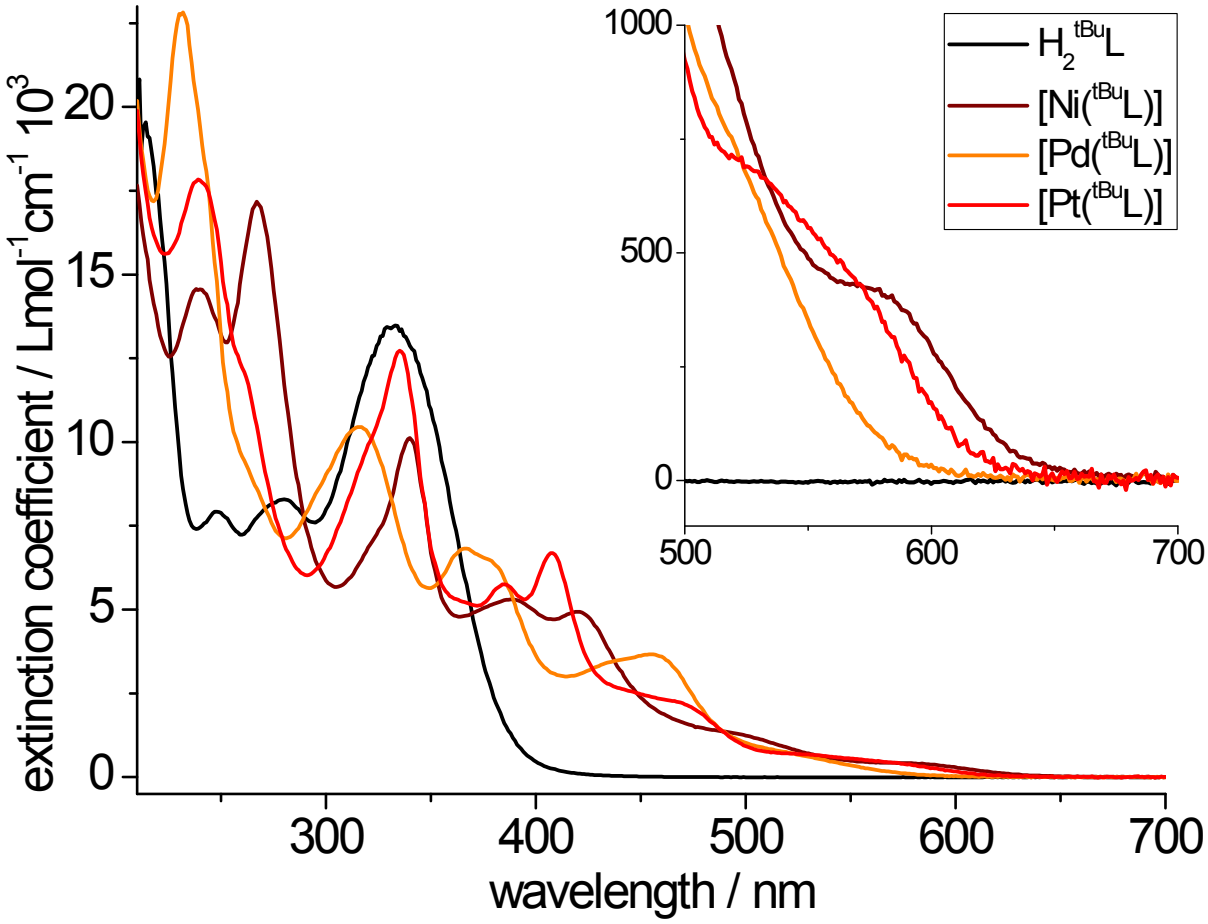

Fig. S24 UV-vis absorption spectra of $\mathbf{H_2^{tBu}L}$ and the complexes **[M(^{tBu}L)]** (M = Pt (red trace), Pd (orange) and Ni (brown).

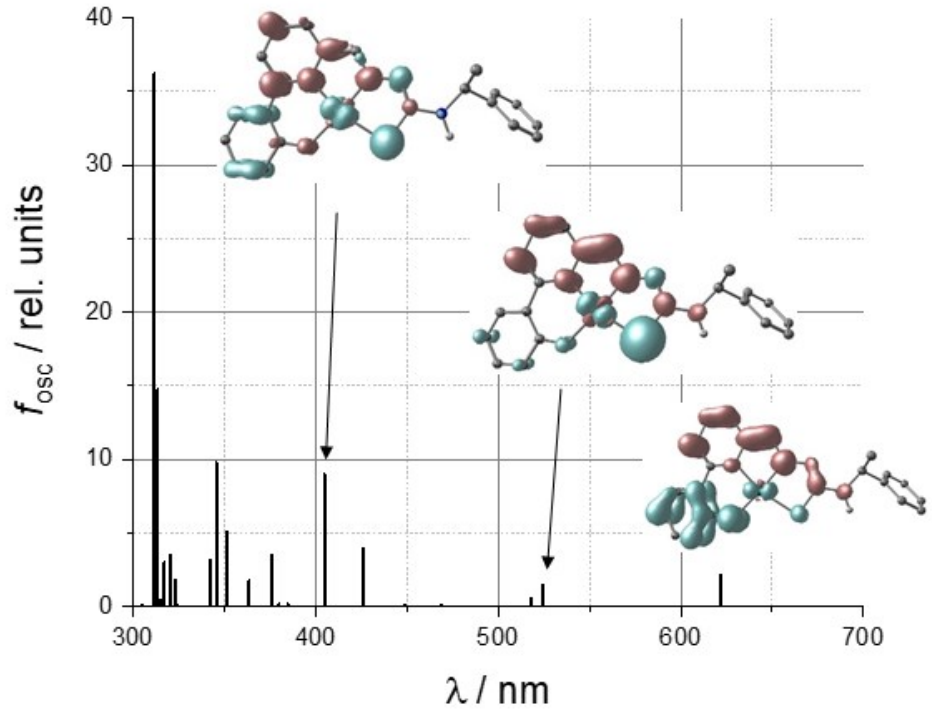

Fig. S25 TD-DFT calculated optical spectrum of **[Pd(L)]**; verticals: transitions. Inset: Difference densities of selected transitions.

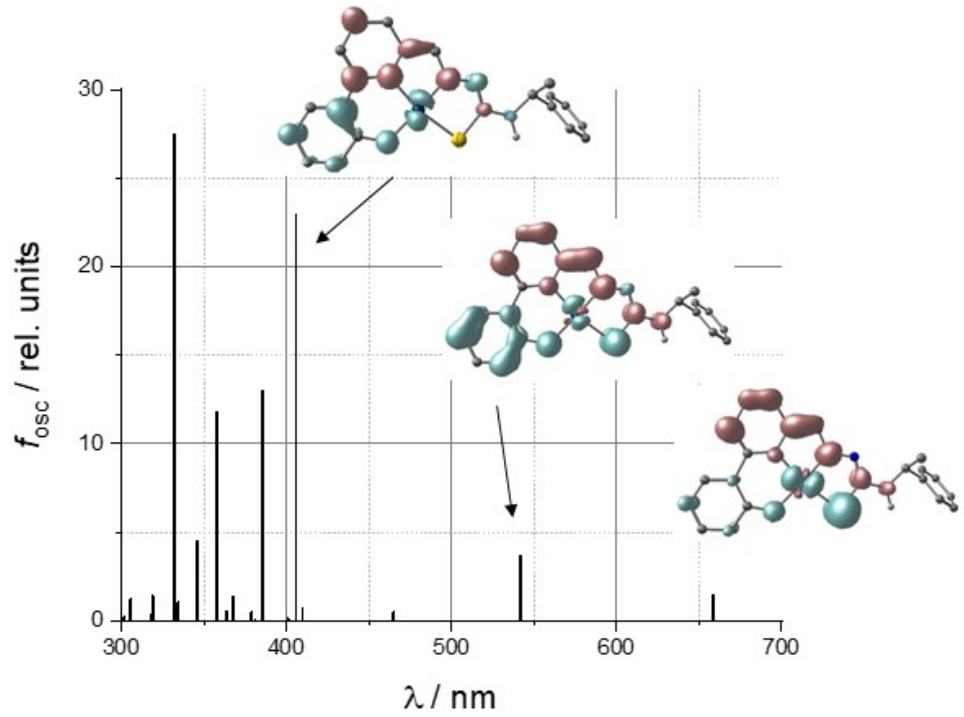

Fig. S26 TD-DFT calculated optical spectrum of **[Pt(L)]**; verticals: transitions. Inset: Difference densities of selected transitions.

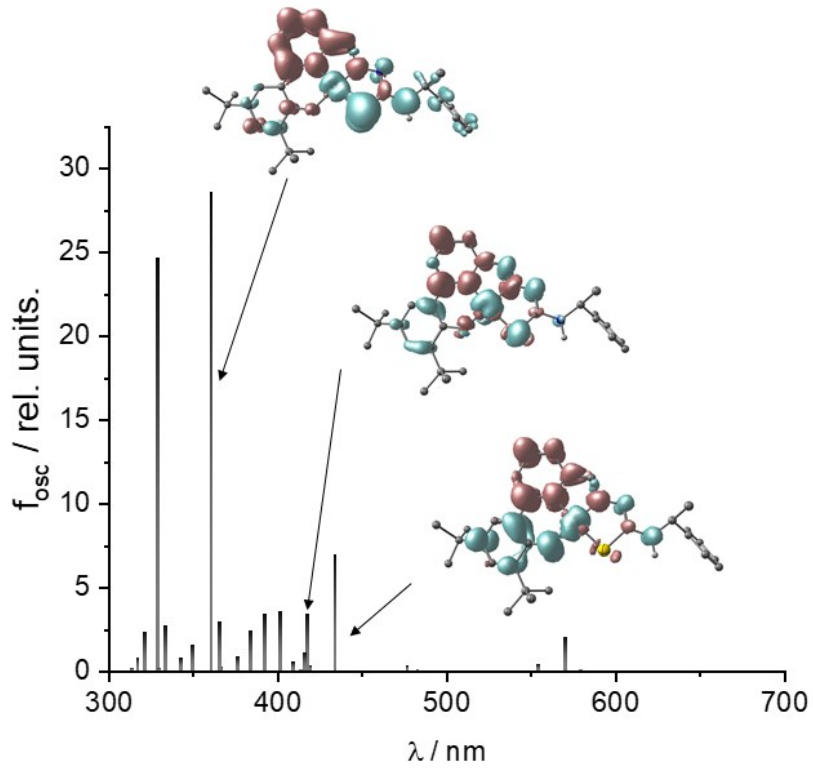

Fig. S27 TD-DFT calculated optical spectrum of **[Ni(^{tBu}L)]**; verticals: transitions. Inset: Difference densities of selected transitions.

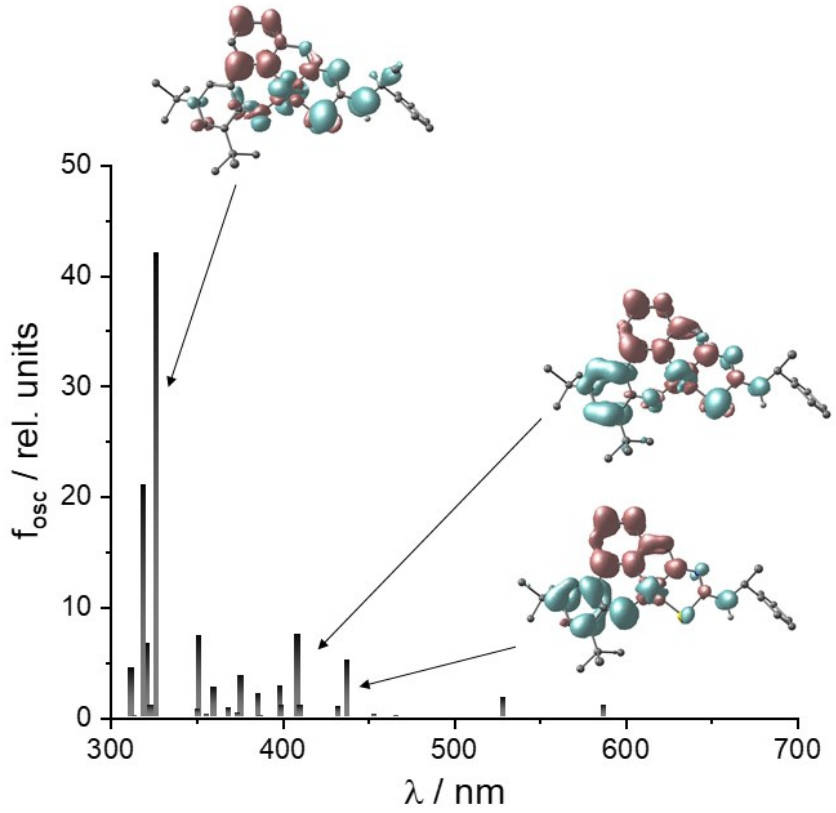

Fig. S28 TD-DFT calculated optical spectrum of **[Pd(^{tBu}L)]**; verticals: transitions. Inset: Difference densities of selected transitions.

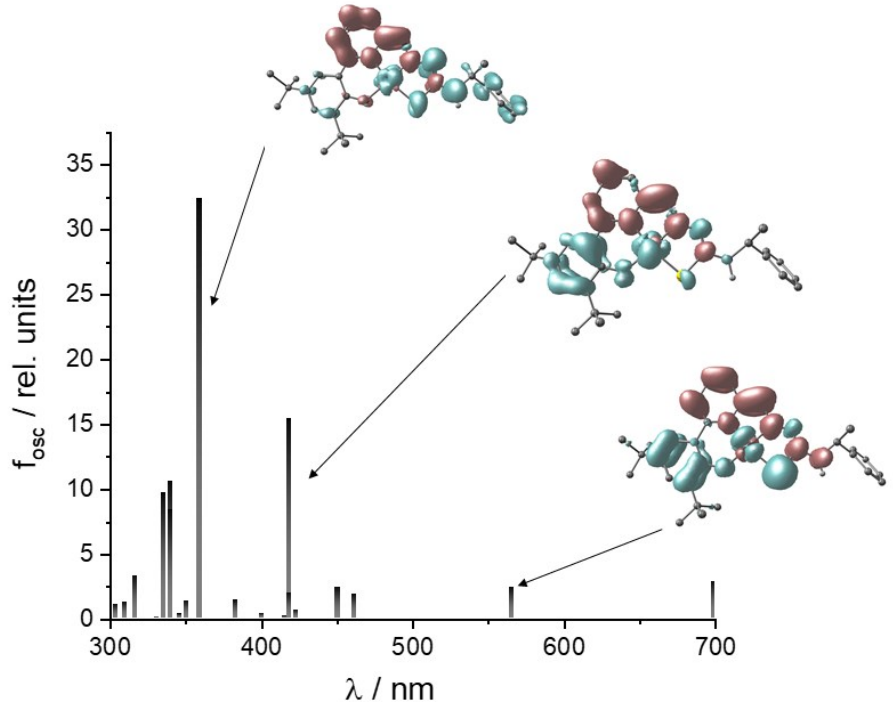

Fig. S29 TD-DFT calculated optical spectrum of **[Pt(tBuL)]**; verticals: transitions. Inset: Difference densities of selected transitions.

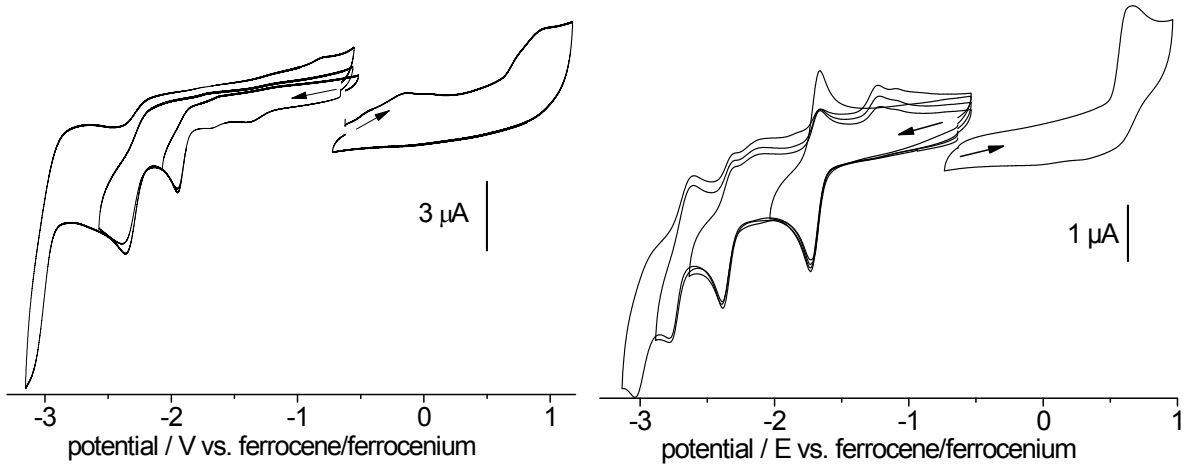

Fig S30 Cyclic voltammograms of H_2L (left) and **[Ni(L)]** (right) in 0.1 M nBu$_4$NPF$_6$ MeCN solution.

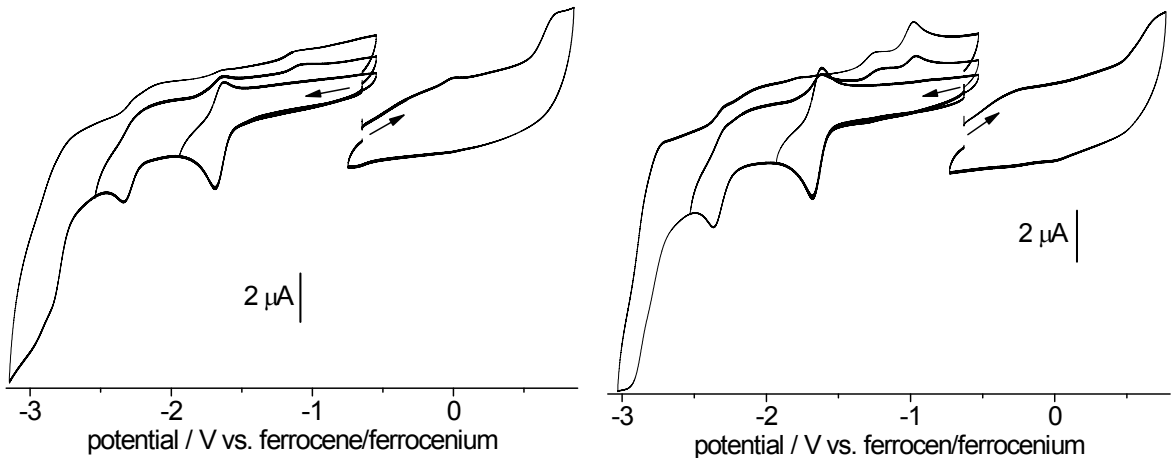

Fig. S31 Cyclic voltammogramms of **[Pd(L)]** (left) and **[Pt(L)]** (right) in 0.1 M n-Bu$_4$NPF$_6$ MeCN solution.

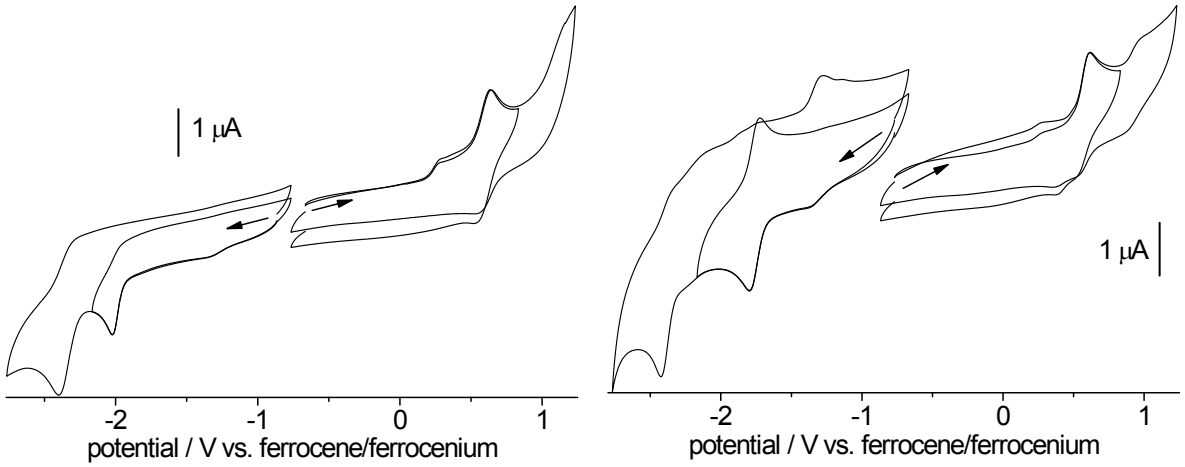

Fig. S32 Cyclic voltammogramms of $\mathbf{H_2}^{\mathbf{tBu}}\mathbf{L}$ (left) and **[Ni(**$^{\mathbf{tBu}}$**L)]** (right) in 0.1 M *n*-Bu_4NPF_6 MeCN solution.

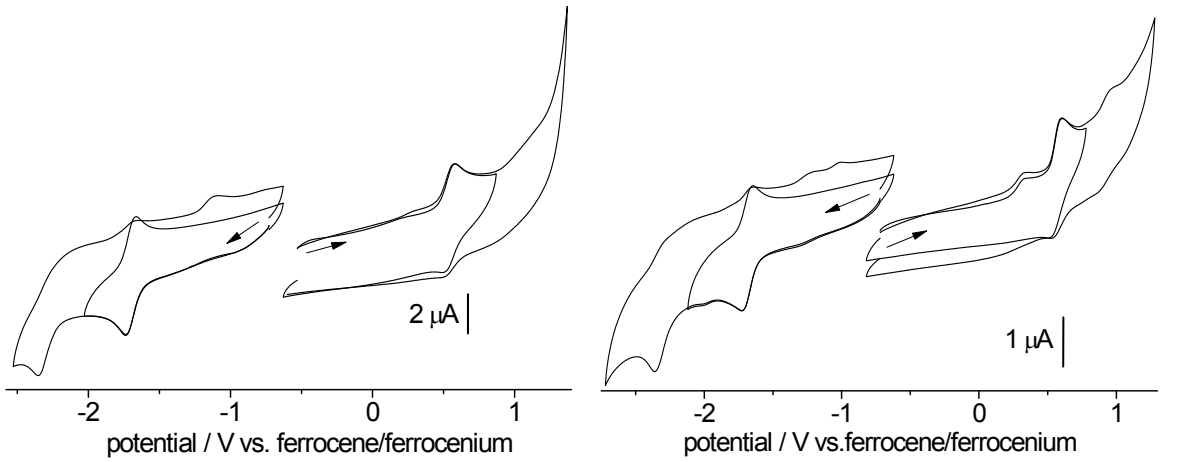

Fig. S33 Cyclic voltammogramms of **[Pd(**$^{\mathbf{tBu}}$**L)]** (left) and **[Pt(**$^{\mathbf{tBu}}$**L)]** (right) in 0.1 M *n*-Bu_4NPF_6 MeCN solution.

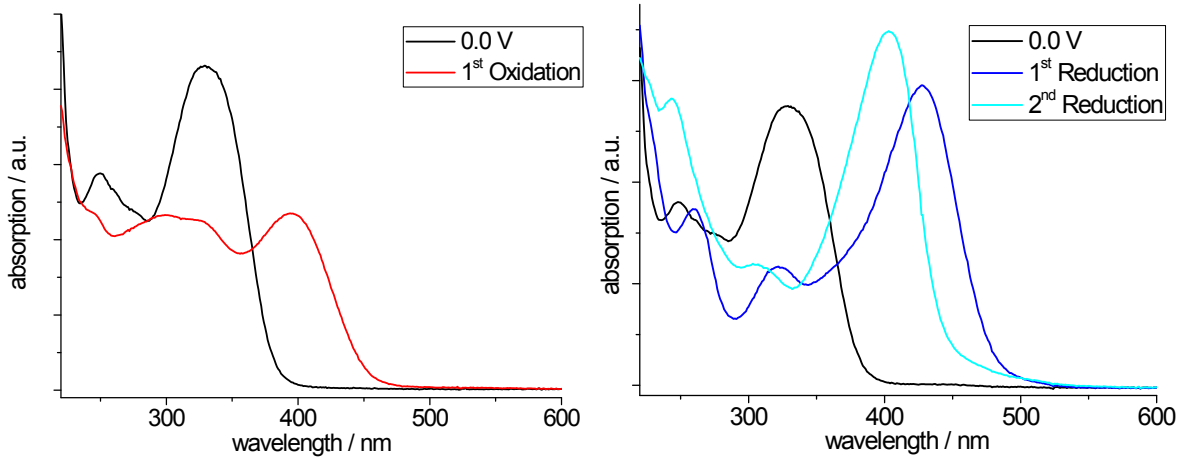

Fig. S34 UV-vis absorption spectra recorded during electrolysis of **HL** in 0.1 M *n*-Bu_4NPF_6 MeCN solution; left: oxidation; right: reductions.

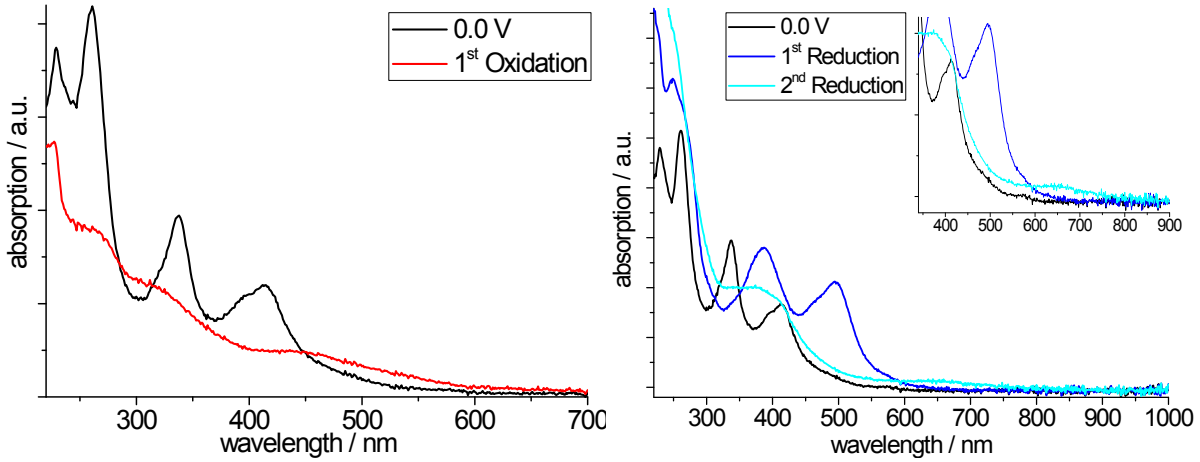

Fig. S35 UV-vis absorption spectra recorded during electrolysis of **[Ni(L)]** in 0.1 M n-Bu_4NPF_6 MeCN solution; left: oxidation; right: reductions.

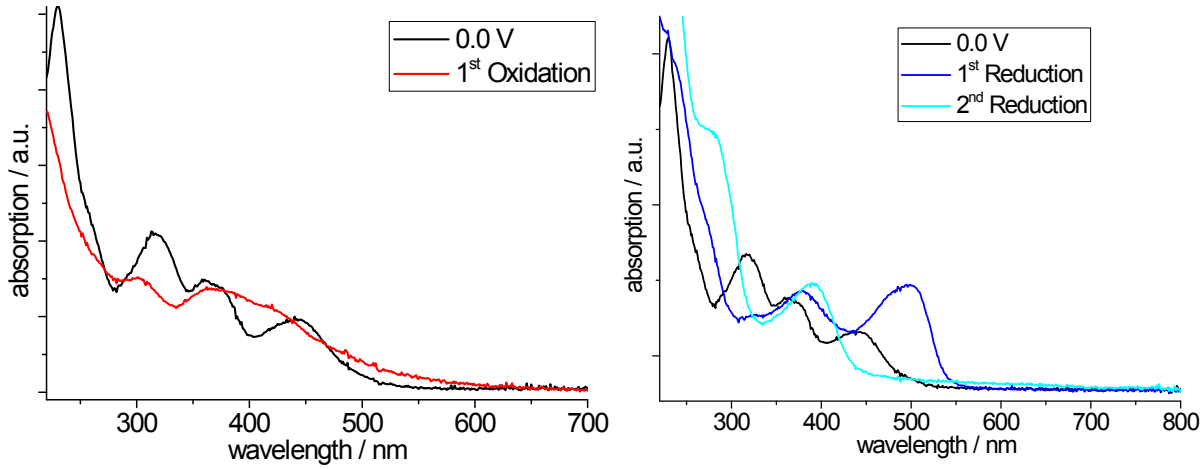

Fig. S36 UV-vis absorption spectra recorded during electrolysis of **[Pd(L)]** in 0.1 M n-Bu_4NPF_6 MeCN solution; left: oxidation; right: reductions.

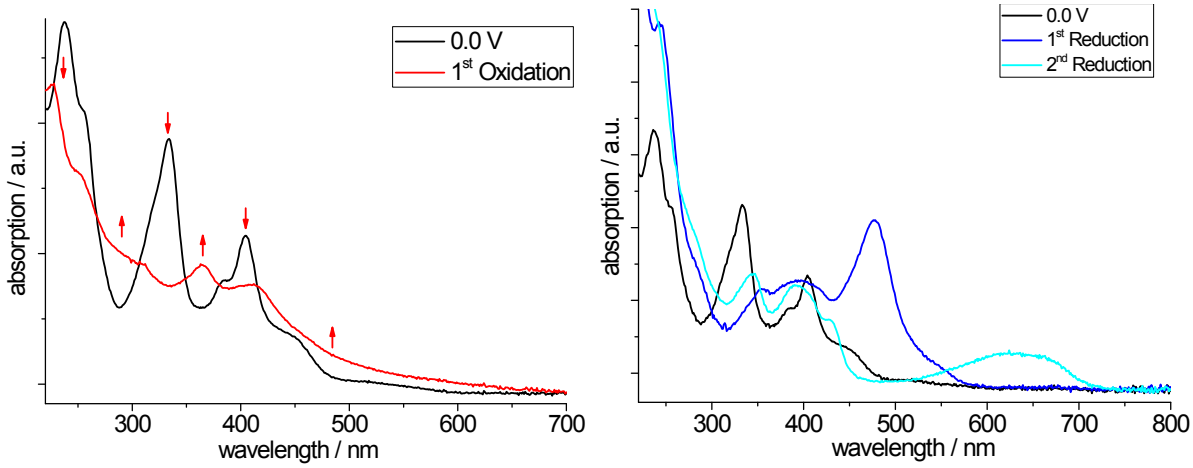

Fig. S37 UV-vis absorption spectra recorded during electrolysis of **[Pt(L)]** in 0.1 M n-Bu_4NPF_6 MeCN solution; left: oxidation; right: reductions.

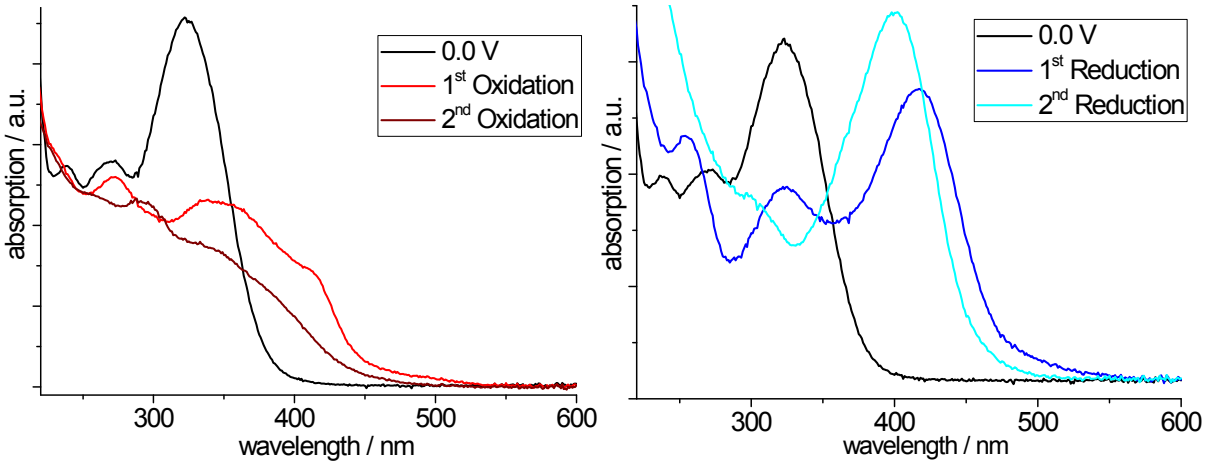

Fig. S38 UV-vis absorption spectra recorded during electrolysis of $\mathbf{H_2{}^{tBu}L}$ in 0.1 M n-Bu_4NPF_6 MeCN solution; left: oxidation; right: reductions.

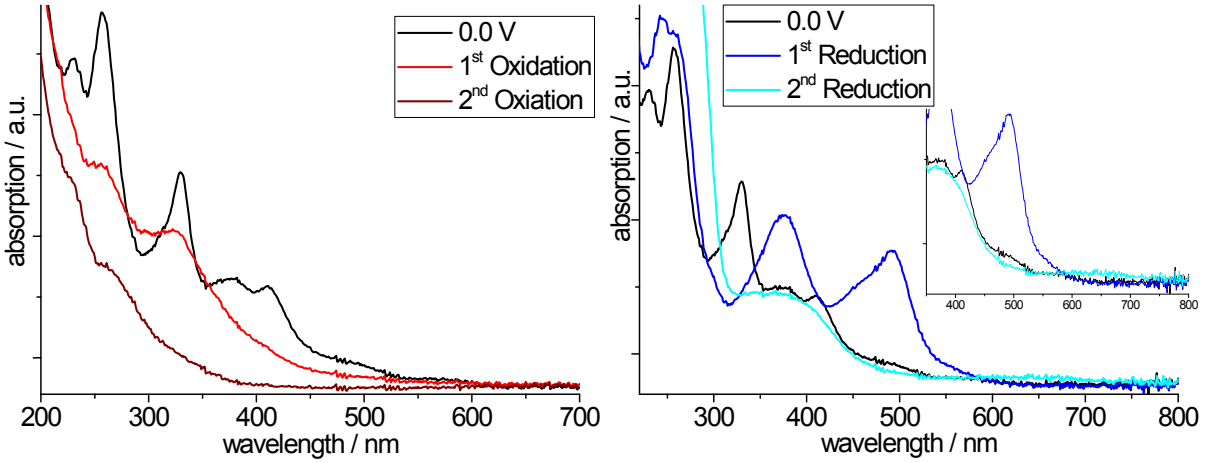

Fig. S39 UV-vis absorption spectra recorded during electrolysis of **[Ni(^{tBu}L)]** in 0.1 M n-Bu_4NPF_6 MeCN solution; left: oxidation; right: reductions.

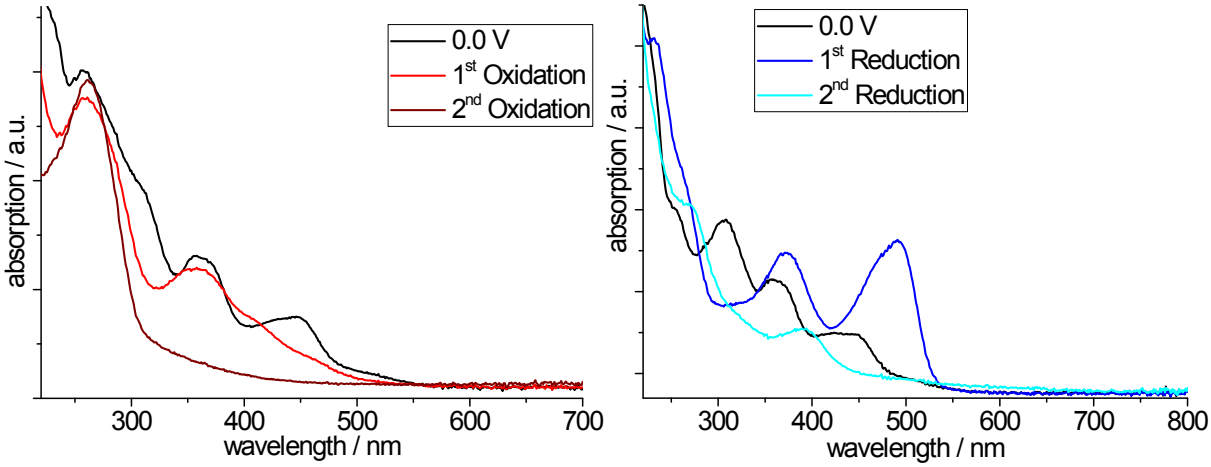

Fig. S40 UV-vis absorption spectra recorded during electrolysis of **[Pd(^{tBu}L)]** in 0.1 M n-Bu_4NPF_6 MeCN solution; left: oxidation; right: reductions.

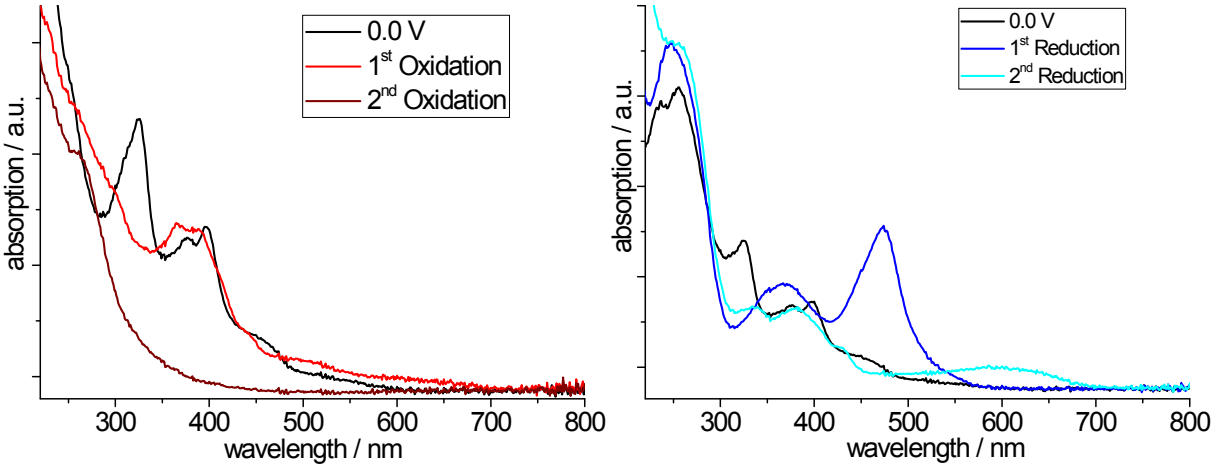

Fig. S41 UV-vis absorption spectra recorded during electrolysis of **[Pt(tBuL)]** in 0.1 M *n*-Bu_4NPF_6 MeCN solution; left: oxidation; right: reductions.

Supporting Tables:

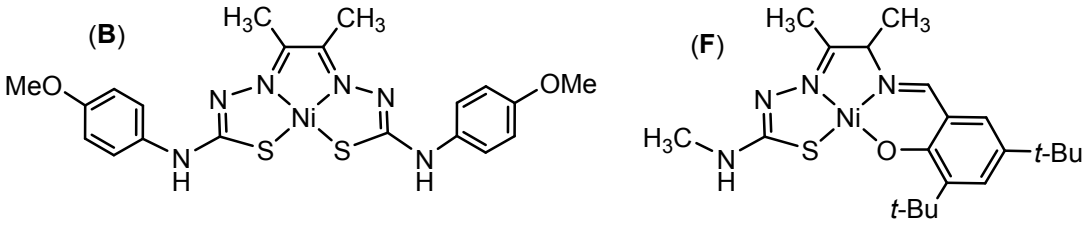

Table S1 Selected DFT calculated structural parameters [a] of the reference Ni(II) complexes **B** and **F;** data in parentheses from single-crystal X-ray crystallography.

	Complex B [b]			**Complex F** [c]
distances / Å			distances / Å	
Ni–S	2.177 (2.170(4) / 2.165(5))		Ni–S	2.194 (2.175(1) / 2.160(2))
Ni–S′	2.180 (2.167(4) / 2.170(5))		Ni–O	1.844 (1.835(2) / 1.833(2))
Ni–N1	1.868 (1.80(1) / 1.82(1))		Ni–N1	1.859 (1.853(3) / 1.847(3))
Ni–N2	1.861 (1.85(1) / 1.84(1))		Ni–N2	1.839 (1.852(3) / 1.844(3))
C–S	1.795		C–S	1.777
C–S′	1.795		C–O	1.314
C–C	1.452		C–C	1.499
angles / °			angles / °	
trans-S′–Ni–N1	171.3		*trans*-S–Ni–N1	172.4
trans-S–Ni–N2	170.9		*trans*-O–Ni–N2	177.9
cis-S–Ni–S′	101.4		*cis*-S–Ni–O	91.4
cis-N–Ni–S	87.7/87.4		*cis*-N–Ni–S	96.1
			N–C–C–C(O)	1.5
			N–C–C–N	9.0

[a] Optimised at the BP86-D3/TZVP/COSMO(THF) level of theory. [b] from ref. [1]. c from ref. [2]. Both complexes contain two independent molecules in the unit cell of the crystal structure.

references:
[1] T. Straistari, J. Fize, S. Shova, M. Réglier, V. Artero and M. Orio, *ChemCatChem* 2017, **9**, 2262–2268.
[2] A. Kochem, G. Gellon, O. Jarjayes, C. Philouze, A. du Moulinet d'Hardemare, M. van Gastel and F. Thomas, *Dalton Trans.*, 2015, **44**, 12743–12756.

Table S2 Computed metrics of the complexes [**M(tBuL)**] (M = Ni, Pd, Pt) and the reference complex **F**;[a]

	F [b,c]	[**Ni(tBuL)**]	[**Pd(tBuL)**]	[**Pt(tBuL)**]
distances / Å				
Ni–S	2.194 (2.175(1))	2.203	2.366	2.318
Ni–O	1.844 (1.835(2))	1.818	2.018	1.981
Ni–N1	1.859 (1.853(3))	1.849	2.004	1.951
Ni–N2	1.839 (1.852(3))	1.875	2.034	2.002
C–S	1.777	1.774	1.785	1.790
C–O	1.314	1.321	1.321	1.329
C–C	1.499	1.434	1.446	1.439
angles / °				
trans-S–Ni–N	172.4	172.1	165.3	167.4
trans-N–Ni–O	177.9	177.1	173.8	176.6
cis-S–Ni–O	91.4	92.1	101.9	98.4
cis-N–Ni–O	96.1	95.7	92.7	94.2
N–C–C–C(O)	1.5	13.3	20.3	14.1
N–C–C–N	9.0	3.1	5.5	3.1

[a] DFT-optimised with BP86-D3/TZVP. [b] For the structure of complex **F** see Scheme 2. [c] Data in parentheses denote experimental metrics reported in ref. 34.

Table S3 Selected DFT calculated structural parameters of **[M(L)]** and **[M(tBuL)]** (M = Ni, Pd or Pt).[a]

	[Ni(L)]	**[Pd(L)]**	**[Pt(L)]**	**[Ni(tBuL)]**	**[Pd(tBuL)]**	**[Pt(tBuL)]**
distances / Å						
Ni–S	2.200	2.364	2.317	2.203	2.366	2.318
Ni–O	1.822	2.022	1.988	1.818	2.018	1.981
Ni–N1	1.849	2.001	1.951	1.849	2.004	1.951
Ni–N2	1.882	2.038	2.008	1.875	2.034	2.002
C–S	1.772	1.784	1.789	1.774	1.785	1.790
C–O	1.321	1.321	1.330	1.321	1.321	1.329
C–C	1.465	1.472	1.472	1.434	1.446	1.439
angles / °						
trans-S2–Ni–N1	172.1	165.3	167.3	172.1	165.3	167.4
trans-O–Ni–N2	177.7	175.2	177.2	177.1	173.8	176.6
cis-S–Ni–O	91.4	101.1	97.9	92.1	101.9	98.4
cis-N–Ni–O	96.5	93.7	94.7	95.7	92.7	94.2
N–C–C–C(O)	0.6	16.0	10.5	13.3	20.3	14.1
N–C–C–N	0.1	3.6	2.1	3.1	5.5	3.1

[a] Optimised at the BP86-D3/TZVP/COSMO(THF) level of theory.

Table S4 Absorption maxima of the protoligands **H2L** and **H2tBuL** and the complexes **[M(L)]** and **[M(tBuL)]** (M = Ni, Pd, Pt) [a]

	λ_1		λ_2		λ_3			λ_4
H_2L	249	274	327					
[Ni(L)]	233	261	337	394	413	450	488	560
[Pd(L)]	229	254	316	360	372	441		497
[Pt(L)]	236	254	333	384	405	444	505	547
$H_2{}^{tBu}L$	248	279	331					
[Ni(^{tBu}L)]	239	267	339		387	420	491	577
[Pd(^{tBu}L)]	231	261	316	366	379	455		518
[Pt(^{tBu}L)]	239	258	335	385	408	468	524	567

[a] Measured in MeCN.

Table S5.1 TD-DFT calculated absorptions of **[Ni(^{tBu}L)]** with f_{osc} > 0.01; character denotes leading orbital contributions.

transition	ν / cm^{-1}	λ / nm	f_{osc}	character
6	14212.5	703.6	0.021	H → L (88 %)
11	17523.5	570.7	0.019	H–1 → L (75 %)
18	23014.8	434.5	0.069	Mixed
20	23935.8	417.8	0.033	Mixed
25	25486	392.4	0.033	Mixed
27	24897.4	401.6	0.035	H–6 → L (30 %) // H–4 → L (40 %)
28	26039	384	0.023	H–6 → L (32 %) // H–4 → L (25 %)
32	27325.9	366	0.029	H–5 → L (43 %)
35	27696.6	361.1	0.285	Mixed
38	28573.8	350	0.015	Mixed
43	29938.8	334	0.026	H–5 → L+1 (43 %)
45	24023.9	416.3	0.010	H–8 → L (84 %)
47	30390.3	329.1	0.246	Mixed
57	31098.6	321.6	0.023	H–4 → L+2 (80 %)
62	33273.7	300.5	0.020	H → L+5 (85 %)
66	34785.7	287.5	0.019	H–10 → L+1 (34 %) // H–5 → L+2 (30 %)
68	33507	298.4	0.035	H–11 → L (42 %) // H–7 → L+1 (47 %)
69	33977	294.3	0.014	H–11 → L (46 %) // H–7 → L+1 (36 %)

Table S5.2 TD-DFT calculated absorptions of **[Pd(^{tBu}L)]** with f_{osc} > 0.01; character denotes leading orbital contributions.

transition	ν / cm^{-1}	λ / nm	f_{osc}	character
3	12886.3	776	0.019	H → L (97 %)
5	17018	587.6	0.010	H → L+1 (95 %)
9	18914.3	528.7	0.017	H–1 → L (74 %)
15	22833.7	437.9	0.051	H–2 → L (28 %) // H → L+1 (51 %)
18	24454.4	408.9	0.075	Mixed
21	25080.8	398.7	0.028	H–2 → L+1 (72 %)
22	25010.2	399.8	0.010	H–5 → L (80 %)
23	26613	375.8	0.037	H–3 → L+1 (72 %)
29	28456.2	351.4	0.073	Mixed
34	27771.5	360.1	0.027	H–8 → L (48 %) // H–6 → L (36 %)
41	30599.2	326.8	0.420	Mixed
43	31092.1	321.6	0.066	Mixed
45	31329.7	319.2	0.209	Mixed
46	24358.3	410.5	0.010	H → L+3 (98 %)
50	32060.6	311.9	0.044	H–9 → L (36 %) // H–8 → L+2 (25 %)
56	25903	386.1	0.020	H–6 → L+2 (98 %)
59	33507.2	298.4	0.032	H → L+5 (52 %)
63	34514.6	289.7	0.041	H–10 → L (61 %)
65	30940.1	323.2	0.010	H–1 → L+3 (92 %)
67	36326.6	275.3	0.022	H–10 → L+1 (80 %)
70	36495.3	274	0.312	Mixed

Table S5.3 TD-DFT calculated absorptions of **[Pt(^{tBu}L)]** with f_{osc} > 0.01; character denotes leading orbital contributions.

transition	ν / cm^{-1}	λ / nm	f_{osc}	character
2	14295.8	699.5	0.028	H → L (93 %)
5	17675.3	565.8	0.023	H–1 → L (85 %)
8	21679.3	461.3	0.018	H → L+1 (89 %)

9	22195.3	450.5	0.024	H–2 → L (77 %)
10	23887.1	418.6	0.153	H–2 → L (45 %)
18	26126.8	382.7	0.014	H–2 → L (52 %)
20	27841.8	359.2	0.324	Mixed
23	23913	418.2	0.019	H–7 → L (91 %)
25	29400.6	340.1	0.106	Mixed
28	29441.2	339.7	0.083	Mixed
30	29784.5	335.7	0.096	Mixed
34	28520	350.6	0.013	H–3 → L+1 (93 %)
42	32305.1	309.5	0.012	H–5 → L+1 (65 %)
44	32964.4	303.4	0.010	H → L+5 (66 %)
54	35643.4	280.6	0.037	Mixed
55	35732.1	279.9	0.036	H–6 → L+1 (40 %)
56	35929.9	278.3	0.159	mixed
58	31589.3	316.6	0.033	H–1 → L+4 (79 %)
65	36432.3	274.5	0.012	H–13 → L (48 %)
68	37678.2	265.4	0.207	mixed

Table S5.4 TD-DFT calculated absorptions of **[Ni(L)]** with f_{osc} > 0.01; character denotes leading orbital contributions.

transition	ν / cm^{-1}	λ / nm	f_{osc}	character
5	15083.7	663	0.012	H → L (87 %)
11	18639.2	536.5	0.029	H–1 → L (82 %)
16	23089.4	433.1	0.017	H → L+2 (67 %)
20	23561.6	424.4	0.082	H–3 → L (48 %)
27	25785.2	387.8	0.018	H–6 → L+1 (46 %)
31	26858.9	372.3	0.036	H–5 → L (56 %)
33	28047	356.5	0.023	Mixed
34	28405.4	352	0.124	Mixed
35	28539.5	350.4	0.087	Mixed
36	29043.8	344.3	0.053	H–8 → L (68 %)
39	29530.9	338.6	0.021	Mixed
42	30819.5	324.5	0.333	Mixed
47	31203.7	320.5	0.011	H–7 → L+2 (36 %) // H–5 → L+2 (26 %)
49	31516.4	317.3	0.027	H–9 → L (74 %)
59	32989.1	303.1	0.010	H–4 → L+2 (55 %)
64	33693.5	296.8	0.040	H → L+5 (80 %)
70	34876.4	286.7	0.027	mixed

Table S5.5 TD-DFT calculated absorptions of **[Pd(L)]** with f_{osc} > 0.01; character denotes leading orbital contributions.

transition	ν / cm^{-1}	λ / nm	f_{osc}	character
3	16087.5	621.6	0.021	H → L (96 %)
5	19081.4	524.1	0.014	H–1 → L (82 %)
14	23475.9	426	0.039	H → L+2 (67 %)
18	24714	404.6	0.09	H–2 → L (40 %) // H–1 → L+2 (35 %)
24	26619	375.7	0.034	H–3 → L+1 (63 %)
26	27520.5	363.4	0.017	H–4 → L (52 %) // H–1 → L+2 (34 %)
28	28470.1	351.2	0.05	H–6 → L (71 %)
30	28925.9	345.7	0.097	Mixed
32	29203.8	342.4	0.031	H–3 → L+2 (74 %)
41	30992.7	322.7	0.018	H–7 → L (94 %)
42	31236.9	320.1	0.035	H–2 → L+2 (68 %)
44	31558	316.9	0.03	H–9 → L (70 %)

48	31903.3	313.4	0.148	H–8 → L (67 %)
49	32104	311.5	0.362	Mixed
57	33695.6	296.8	0.02	H–1 → L+3 (88 %)
58	33760	296.2	0.109	H–10 → L (48 %)
59	34192.8	292.5	0.035	H → L+5 (50 %)
67	36184.9	276.4	0.035	H–7 → L+1 (88 %)
68	36273.6	275.7	0.044	H–10 → L+1 (62 %)
69	36456.3	274.3	0.075	Mixed
72	36890.4	271.1	0.061	H–6 → L+2 (43 %)
74	37036.9	270	0.017	H–2 → L+3 (96 %)

Table S5.6 TD-DFT calculated absorptions of **[Pt(L)]** with f_{osc} > 0.01; character denotes leading orbital contributions.

transition	ν / cm^{-1}	λ / nm	f_{osc}	character
2	15092.2	662.6	0.015	H → L (92 %)
5	18968.9	527.2	0.034	H–1 → L (87 %)
12	24392.1	410	0.151	H–2 → L (46 %)
18	28003.1	357.1	0.046	H–5 → L (40 %)
20	29085.9	343.8	0.185	Mixed
24	29553.2	338.4	0.082	H–3 → L+1 (40 %)
26	29784.3	335.7	0.092	Mixed
27	29981.5	333.5	0.057	Mixed
28	30023	333.1	0.017	Mixed
30	30643.6	326.3	0.208	Mixed
35	31314.5	319.3	0.033	H–7 → L (90 %)
49	34354.1	291.1	0.034	Mixed
51	34539.9	289.5	0.014	H–1 → L+3 (50 %)
54	35425.4	282.3	0.063	H–6 → L+1 (74 %)
57	36112.9	276.9	0.083	Mixed
59	36277	275.7	0.034	H–2 → L+2 (76 %)
63	37192.5	268.9	0.079	H–3 → L+4 (56 %)
65	37434	267.1	0.017	H–2 → L+4 (50 %)
66	37454	267	0.17	Mixed

Table S6 Selected electrochemical data of the protoligands **H_2L** and **H_2t^{Bu}L** and the complexes **[M(L)]** and **[M(t^{Bu}L)]** (M = Ni, Pd, Pt) [a]

	$E_{1/2Red3}$	$E_{1/2Red2}$	$E_{1/2Red1}$	$E_{1/2Ox1}$	E_{paOx2}	$\Delta E_{Ox1–Red1}$	$\Delta E_{Red1–Red2}$
H_2L	–3.12 irr	–2.36 *irr*	–1.94 *irr*	0.94 *irr*		2.88	0.42
[Ni(L)]	–2.72	–2.37	–1.70	0.66 *irr*		2.36	0.67
[Pd(L)]	–2.97 irr	–2.34	–1.66	0.72 *irr*		2.38	0.68
[Pt(L)]	–2.93 irr	–2.36	–1.65	0.69 *irr*		2.34	0.71
H_2t^{Bu}L		–2.40 *irr*	–2.02 *irr*	0.59	1.14 *irr*	2.61	0.38
[Ni(t^{Bu}L)]		–2.42	–1.75	0.56	0.99 *irr*	2.31	0.67
[Pd(t^{Bu}L)]	–2.88 irr	–2.35	–1.70	0.55	>1.15	2.25	0.65
[Pt(t^{Bu}L)]		–2.36	–1.69	0.55	0.97 *irr*	2.24	0.67

[a] From cyclic voltammetry, electrochemical potentials in V (uncertainties ~1-3 mV), half-wave potentials $E_{1/2}$ for reversible and partially reversible redox waves and peak potentials E_{pc} or E_{pa} for irreversible (*irr*) waves; measured in 0.1 M nBu$_4$NPF$_6$/MeCN at 298 K, scan rate 100 mV/s.